J. Fluid Mech. (1976), *vol.* 73, *part* 2, *pp.* 265–304
Printed in Great Britain

The turbulence structure of a highly curved mixing layer

By I. P. CASTRO† AND P. BRADSHAW
Department of Aeronautics, Imperial College, London

(Received 21 November 1974 and in revised form 7 April 1975)

As part of a general investigation of complex turbulent flows, extensive one-point measurements have been made of the turbulence structure of the mixing layer bounding a normally impinging plane jet with an irrotational core. The ratio of shear-layer thickness to streamline radius of curvature reaches a maximum of about 0·2, the sense of the curvature being stabilizing. Downstream of the impingement region the shear layer returns asymptotically to being a classical plane mixing layer. The most striking feature of the results is that the return is not monotonic: after decreasing in the region of stabilizing curvature, the Reynolds stresses, triple products, energy dissipation rate and other turbulence quantities overshoot the plane-layer values before finally decreasing. Some conclusions are drawn about the nature of the turbulent transport of Reynolds stress, and about the representation of this and other processes in calculation methods for complex turbulent flows. An incidental result of the work is a comprehensive set of measurements in a *plane* mixing layer.

1. Introduction

Because turbulent stresses are so small compared with typical dynamic pressures, turbulent stress gradients significantly affect the development of a flow only if the stress changes by a large fraction in a small distance. The Reynolds-stress transport equations generally preclude rapid changes of stress along mean streamlines, so that any large gradients are usually in the direction normal to the streamlines. The stress whose gradient normal to a given line affects the flow along that line is a shear stress (referred to the given line and its normal as axes). There follows the well-known conclusion, valid also for laminar flow at high Reynolds number, that nearly all flows with significant stress gradients are fairly thin shear layers, whose thickness δ is one or more orders of magnitude smaller than the streamwise distance l from the shear-layer origin. If the shear layer is to remain fairly thin, the basic rate of shear strain, $\partial U/\partial y$ in the usual notation, must be much larger than any extra rate of strain in some other direction, e say, tending to distort the layer. If this inequality is strong enough, i.e. if $e(\partial U/\partial y)^{-1} \ll 1$ or $\delta/l \ll 1$, some terms in the equations of motion are small enough to be neglected and we arrive at Prandtl's thin-shear-layer ('boundary layer') approximation. The above reasoning has led some authors to suppose that the thin-shear-layer

† Present address: Central Electricity Generating Board, Marchwood Engineering Laboratories, Marchwood, Southampton, England.

Name	Inequality	Effect of extra strain rate on turbulence structure
Simple shear layer	$10e(\partial U/\partial y)^{-1} \ll 1$	Negligible
Thin shear layer	$e(\partial U/\partial y)^{-1} \ll 1$	Possibly significant
Fairly thin shear layer	$10e(\partial U/\partial y)^{-1} < 1$	Probably large

TABLE 1. Classification of shear layers by ratio of extra strain rate to mean shear: the symbol $\ll$ denotes a factor of inequality not much less than 100.

approximation, and even any calculation method which is successful in shear layers, can be applied with sufficient accuracy to nearly all flows with significant stress gradients. This assumption has been made, for instance, in a number of calculation methods for supersonic separated flows. However there are many shear layers which, although *fairly* thin, do not everywhere satisfy the requirements of the thin-shear-layer approximation $e(\partial U/\partial y)^{-1} \ll 1$. Also, evidence is rapidly accumulating that the effect of extra rates of strain on the turbulence structure of a shear layer is often surprisingly large, producing fractional changes in Reynolds stress of the order of $10\,e(\partial U/\partial y)^{-1}$, which can be significant even if the thin-shear-layer approximation is obeyed. We need to distinguish different classes of shear layer according to typical values of $e(\partial U/\partial y)^{-1}$, and a suggested classification in order of increasing size of extra strain rate is given in table 1: for a fuller discussion see Bradshaw (1973). Only a few slowly growing undistorted flows will satisfy the 'simple shear layer' requirement that the effects of any extra strain rates on turbulence structure shall be small. Note that a mere change in $\partial U/\partial y$ is *not* regarded as an 'extra' rate of strain: it does not affect the validity of the thin-shear-layer approximation and its effect on the turbulence structure is not unexpectedly large because it is the response to $\partial U/\partial y$ that conditions our expectations.

According to the above reasoning, nearly all flows with significant Reynolds-stress gradients should satisfy the 'fairly thin shear layer' requirement, very roughly $e(\partial U/\partial y)^{-1} < 0{\cdot}1$, except perhaps for localized regions of strong distortion where pressure gradients overwhelm Reynolds-stress gradients. We must expect the turbulence structure of 'fairly thin shear layers' to be greatly affected by extra strain rates: in particular, localized regions of strong distortion may affect the turbulence structure for some distance downstream.

This paper is one of a series on 'complex' turbulent flows (defined as shear layers with complicating influences like extra strain rates or interactions with other shear layers). The object of this research is to document the effect of these complicating influences so that some of the calculation methods which have proved satisfactory in simple shear layers can be extended with some confidence to complex flows. An introduction was given by Bradshaw (1971*a*) and a progress report by Bradshaw (1975). Broadly speaking the work has shown that the effect on the turbulence structure of interaction with another parallel shear layer is small (Bradshaw, Dean & McEligot 1973; Morel, Torda & Bradshaw 1973; Dean 1974*a*, *b*) but has confirmed the findings of other authors that the effects of extra

strain rates on turbulence structure are very large (Bradshaw & Wong 1972; Bradshaw 1974; Meroney 1974; Brederode & Bradshaw 1974; Young 1974, unpublished work at Imperial College). Progress with calculation methods was described by Bradshaw & Unsworth (1973, 1974): we have assumed that, in general, methods based on the Reynolds-stress transport equations will be needed in complex flows.

The large effect of streamline curvature in the plane of the mean shear ($e = \partial V/\partial x$) has been rediscovered at intervals over the last 40 years at least and is now generally known: for a detailed review see Bradshaw (1973). Qualitatively at least, the effect of streamline curvature is similar to that of buoyancy. A quantitative, though necessarily inexact, analogy has been drawn by Prandtl (see Tollmien, Schlichting & Görtler 1961), Bradshaw (1969) and others: analogues of buoyancy parameters such as the Richardson number can be defined for curved flows and correlations of buoyancy effects in the atmospheric inner layer can be used with tolerable accuracy to predict the effects of mild and prolonged curvature in laboratory wall layers (e.g. Meroney 1974). More complicated cases such as the present one do not correspond to any realizable buoyant flow but the analogy is still useful in general terms. Both buoyancy and curvature produce the surprisingly large changes in Reynolds stress referred to above, an order of magnitude larger than expected from the size of the explicit extra 'generation' terms in the Reynolds-stress transport equations; the size of the existing terms is changed by the extra strain rate or body force although they do not contain it explicitly. Eddy-viscosity and mixing-length formulae, which can be derived as local-equilibrium approximations to the transport equations, also underpredict the effects: an isotropic eddy-viscosity formula predicts that the change in Reynolds stress produced by an extra strain rate e is $e(\partial U/\partial y)^{-1}$ times the Reynolds shear stress $-\rho\overline{uv}$, whereas the actual factor is of the order of $10e(\partial U/\partial y)^{-1}$. Clearly this apparent order-of-magnitude amplification of the extra terms in the transport equations cannot continue when $e(\partial U/\partial y)^{-1}$ is more than about 0·1, or mean-square intensities or energy dissipation rates would become negative. It is well known that highly stable buoyant flows revert to a non-turbulent state while highly unstable ones develop penetrative convection, which replaces true Reynolds stresses as the primary agent of momentum transfer in the vertical direction: similar gross changes must be expected in highly curved flows at the upper limits of the 'fairly thin shear layer' range in table 1.

Highly curved flows close to a state of self-preservation have been studied by a number of authors, such as Giles, Hayes & Sawyer (1966), Guitton (1970) and others in wall jets, Lumley and colleagues (see Wyngaard *et al.* 1968) in a mixing layer, and So & Mellor (1972, 1973) in a boundary layer. These experiments were reviewed by Bradshaw (1973) and only their directly relevant features will be mentioned here. The work of Wyngaard *et al.* is most relevant to the present mixing-layer study, being also the only one of the previous experiments to document one of the Reynolds-stress transport equations (the turbulent energy equation), but measurements were presented at one station only and the turbulent energy balance implies an improbable behaviour of the pressure 'diffusion' term. So & Mellor's measurements showed a very rapid decrease in shear stress

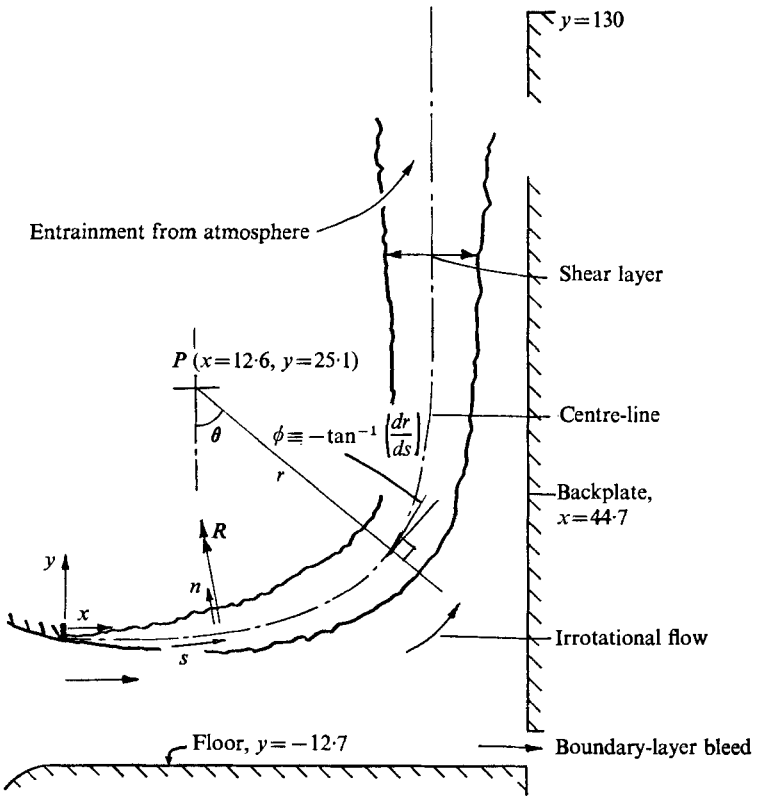

FIGURE 1. Flow geometry and notation: all dimensions in cm. Fixed point P is near, but not at, centre of curvature: the latter varies with s.

after the start of a region of stabilizing curvature, subsequent changes being slow, but they did not make enough measurements to extract an energy balance. We decided that one of the most useful flows for developing and testing calculation methods would be the strongest possible perturbation of an initially self-preserving shear layer with a subsequent return to the same self-preserving state: both end states would be clearly defined and, with sufficiently detailed measurements, the effect of curvature history would be assessable.

The configuration chosen for the present experiments is shown in figure 1; the maximum value of $\partial V/\partial x$ in the central region of the mixing layer is about $-0{\cdot}2\partial U/\partial y$ (using x, y axes aligned with the local direction of the shear layer) so that the 'fairly thin shear layer' limit is exceeded for a short streamwise distance only. The flow can be thought of as half a two-dimensional impinging jet, with a potential core; the 'floor' replaces the plane of symmetry. It was chosen as the only obvious case of a monotonic shear layer (i.e. one with mean shear of the same sign everywhere) which could be strongly perturbed by a short region of large curvature without the occurrence of a change of species (e.g. a change from a free jet to a wall jet or from a boundary layer to a separated shear layer). Two disadvantages of the present configuration are that only a stabilizing sense of streamline curvature can be obtained and that the mixing layer merges with the

boundary layer on the impingement surface before relaxation to the self-preserving state is complete. The second disadvantage is minor, since we documented the self-preserving plane mixing layer in a companion experiment; the first is outweighed by the clarity with which (stabilizing) curvature effects are demonstrated by this flow, and by the practical importance of impinging jet flows.

The measurements presented here were intended to document the transport equations for turbulent energy and shear stress as fully as possible, and include the triple products that effect turbulent transport of shear stress and turbulent energy. We have not measured any quantities involving pressure fluctuations, and our deductions of energy dissipation rates from frequency spectra may not be absolutely reliable although they should be adequate for comparative purposes. The unmeasured pressure–strain 'redistribution' term in the shear-stress transport equation can be deduced as the difference in the measured terms if transport by pressure fluctuations can be neglected: this neglect seems to be justified *a posteriori* except near the high velocity edge of the curved shear layer. So far, only one-point measurements have been made, but the results emphasize the need for correlation measurements to provide information about eddy length scales.

The most spectacular feature of the measurements is that the Reynolds stresses and other turbulent quantities, after decreasing as expected in the region of high stabilizing curvature, rise rapidly further downstream and overshoot the plane-layer values before finally decreasing. The measurements could not be extended far enough downstream to be absolutely sure that the final decrease to the plane-layer values was monotonic, but any further oscillations would surely be very slight. We have of course checked carefully that the overshoot in Reynolds stress was not caused by low frequency 'flapping' unsteadiness of the shear layer in the plane of the mean shear, rather than true turbulence: the simplest proofs that no such unsteadiness occurred are the presence of an overshoot in the spanwise-component intensity and the absence of very low frequency humps in the streamwise-component spectra. It appears that the main reason for the overshoot is that the large eddies, which effect turbulent transport from the high intensity region towards the edge of the shear layer, re-establish themselves rather more slowly after the curvature ends than does the rest of the energy-containing turbulence. It may also be that, like turbulence in the later stages of transition, the re-established turbulence is more 'efficient' than ordinary turbulence, in the sense that it can carry more Reynolds stress for a given dissipation rate. However one would expect 'efficient' shear-layer turbulence to have a higher ratio of shear stress to turbulent intensity than usual, and this is not observed.

It will emerge during the discussion below that the present results undermine many of the principles used in current calculation methods for shear layers, such as the automatic use of the shear-layer thickness to provide a length scale, the rotational invariance of turbulence models based on second-order transport equations, and the gradient-diffusion hypothesis for turbulent transport. These principles are also undermined by physical arguments. Where possible we have suggested alternative principles and tested them against the present results.

2. Apparatus and techniques

The rig shown in figure 1 was attached to the exit nozzle of a 30×5 in. ($7{\cdot}6 \times 12{\cdot}7$ cm) blower tunnel. The tunnel turbulence level, measured within a conventional working section, was less than $0{\cdot}09\,\%$ at the exit speed, U_{ref} or U_r, of $100\,\mathrm{ft/s^{-1}}$ ($33\,\mathrm{m\,s^{-1}}$) used in the present experiments. Measurements in a plane mixing layer at the same tunnel speed, presented in detail by Castro (1973), showed that mean velocity profiles were accurately self-preserving for $x > 20\,\mathrm{cm}$ ($U_{\mathrm{ref}}x/\nu = 4 \times 10^5$, $x/\theta_0 \simeq 700$)† with a spreading parameter σ of 11·1, close to the value of 11·3 found by Liepmann & Laufer (1947) but very different from the value of 9 reported by Wygnanski & Fiedler (1970). Observations of smoke at flow speeds of less than $1\,\mathrm{m\,s^{-1}}$ showed the formation and multiple pairing of spanwise 'vortices' in the unstable laminar flow but the pairing soon became helical and a wholly three-dimensional turbulence pattern ensued. We believe that the mixing layer at $U_{\mathrm{ref}} = 33\,\mathrm{m\,s^{-1}}$, $x > 20\,\mathrm{cm}$ was typical of high Reynolds number flows and did not have the strongly periodic and presumably two-dimensional structure found at low Reynolds numbers by Winant & Browand (1974) and at moderate Reynolds numbers by Brown & Roshko (1974). There is some evidence (Chandrsuda & Bradshaw 1975) that the periodicity found by Brown & Roshko was exaggerated by the spanwise-integrating properties of their shadowgraph technique and the low aspect ratio of their test rig. The large-eddy motions in a mixing layer are undoubtedly very vigorous, but the extensive correlation measurements of Bradshaw, Ferriss & Johnson (1964) and Weber (1974) show that they are three-dimensional, while frequency spectra show broad peaks covering several octaves: the large-scale motion therefore appears to be what is commonly called turbulence rather than a deterministic instability mode. The contrary conclusions in the literature appear to be based on low Reynolds number flows subject to the notoriously prolonged effects of transition, accentuated in some cases by interaction with the columnar instability of circular jets.

The ratio of the distance of the nozzle from the impingement surface, 4·47 cm, to the height of the nozzle opening, 12·7 cm, was chosen such that the core of irrotational flow would not be completely entrained by the shear layer until well after the end of the curved region. Boundary-layer separation in the corner between the floor and the impingement surface (the 'backplate' in figure 1) was suppressed by allowing a volume flow of air equal to about $4U_{\mathrm{ref}}\,\mathrm{cm^3\,s^{-1}}$ per unit span to escape through a slot in the corner running the full width of the test rig. As a result, the potential-flow streamlines cannot be calculated from the rig geometry, and a reference streamline was therefore measured. An electrically heated wire was fixed along a spanwise line 4 cm below the upper lip of the nozzle ($y = -4$ cm in figure 1) and the path of the streamline starting at the wire was traced by traversing a thermocouple normal to the heated wake. This streamline remains in the potential flow until after the end of the curved region, and thereafter the backplate surface was used as the reference streamline. Two-dimensionality of the shear layer was checked by measuring the spanwise

† Here θ_0 is the initial momentum thickness.

distance between the thermal wakes of two heated wires set normal to the plane of the layer near the nozzle lip. The flow diverged slightly: a pessimistic estimate of the apparent origin of lateral divergence was about 20 m upstream of the nozzle lip, corresponding to an error in momentum balance of no more than 3%, and divergence was therefore ignored in analysing the results.

Standard hot-wire techniques were used, with DISA 55D01 constant-temperature anemometers, 55F01 single-wire probes and 55A38 cross-wire probes. Probes were individually calibrated for response to the magnitude and direction of the velocity. The yaw calibrations of the cross-wire probes were expressed as the apparent angle between the wire and the stream, deduced from the calibration by assuming that the wire responded only to the velocity component normal to itself. In effect, this fits the yaw calibration by a cosine curve with the same slope over the (small) range of calibration and uses the cosine as a plausible extrapolation (Bradshaw 1971*b*, pp. 121 ff.). The geometrical angle of the wire is not required. The problems of yaw calibration are discussed at greater length by Castro (1973), where it is concluded that the inevitable inaccuracies resulting from the inability of a 45° wire to distinguish between flow angles of $45-\theta$ and $45+\theta$ render the use of calibrations more elaborate than the 'effective cosine' law rather unrealistic.

Except for the mean-flow and u-component spectrum measurements, all hot-wire signals were recorded on analog magnetic tapes (which are still available) and later transferred to digital tape by the data logger described by Brandt & Bradshaw (1972). The effective sampling rate was 10 kHz although not every point was used in the subsequent data analysis; the presence of power in the spectrum above the Nyquist frequency (half the sampling rate) introduces errors only in statistical quantities involving the time domain, and conventional mean products of any order are unaffected. The digital tapes were analysed on the Imperial College CDC 6400 computer, using adaptations of the program described by Brandt & Bradshaw: linearization of hot-wire signals was carried out in the computer, and the total computing time for evaluation of products and cross-products of up to fourth order from cross-wire signals at one point in the flow was about three times the analog sampling time of roughly 20 s.

The digital processing techniques are straightforward, with the exception of the determination of the intermittency. The problems that appear in the latter – problems which are largely ignored by the 'eyeball' process of finding intermittency from oscilloscope traces and suppressed by the heavily damped analog intermittency meters used by many workers in the past – are discussed in more detail by Castro (1973) and Bradshaw & Murlis (1974). In the present work the flow was declared turbulent when $\partial(uv)/\partial t$ *or* $\partial^2(uv)/\partial t^2$ exceeded a chosen threshold value, ignoring turbulent or irrotational intervals of less than two digital sampling intervals (0·2 ms, or a distance of 0·40 cm in the maximum-intensity region, where $U \simeq 20\,\mathrm{m\,s^{-1}}$). Measurements in a boundary layer by Murlis (unpublished) show that the probability density of 'burst' length rises monotonically as the burst length decreases, at least down to the shortest

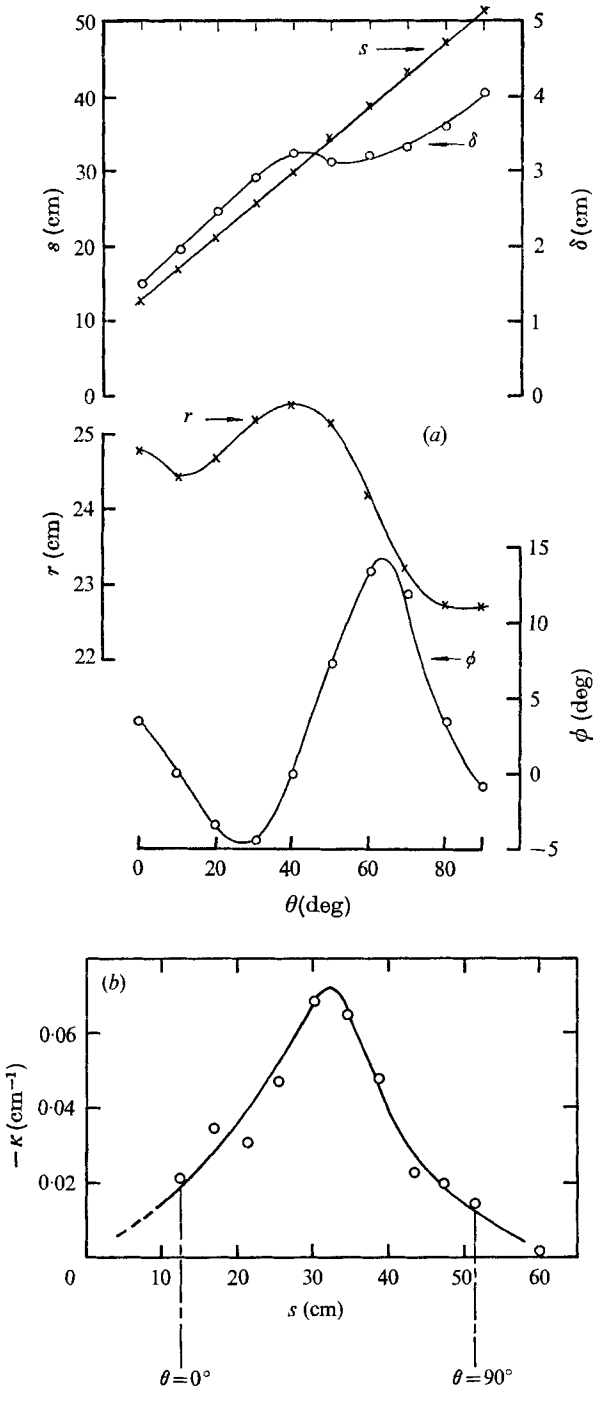

FIGURES 2 (*a*, *b*). For legend see facing page.

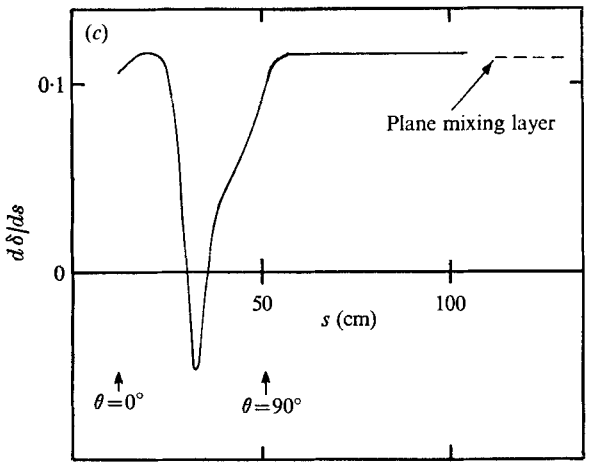

FIGURE 2. Centre-line geometry and shear-layer thickness. (*a*) Variation with polar co-ordinate angle θ; for $60 < s < 100$, $\delta = 0{\cdot}115s - 1{\cdot}728$; $\phi \equiv \tan^{-1}(dr/ds)$. (*b*) Variation of centre-line curvature $\kappa = 1/R$ with distance s round centre-line. (*c*) Rate of growth of shear-layer thickness.

measurable length: deductions about an 'average burst length' are therefore essentially unreliable and are not attempted here.

The turbulent energy dissipation ϵ on the centre-line was deduced from fits of the universal-equilibrium spectrum data of Grant, Stewart & Moilliet (1962) to u-component frequency spectra, measured by analog techniques and corrected for hot-wire length effects by the method of Wyngaard (1968): values of ϵ off the centre-line were deduced by assuming that ϵ is proportional to $(\overline{q^2})^{\frac{3}{2}}$ on a given profile, so that the dissipation length scale $L_\epsilon \equiv (\overline{q^2})^{\frac{3}{2}}/\epsilon$ is constant across the width of the layer. L_ϵ appears to be very nearly independent of y in the measurements of Liepmann & Laufer (1974) in a plane mixing layer, and the above technique gave satisfactory results in our own plane layer. Frequency spectra off the centre-line of the curved layer did not contain any significant region with the $-\frac{5}{3}$-power law expected in an inertial subrange, and dissipation values extracted by making plausible allowances for the effects of intermittency and departures from Taylor's hypothesis were implausible. These eccentricities did not seem to be attributable to curvature effects (no spectra were measured off the centre-line of the plane layer) nor to an excessively low Reynolds number, the microscale Reynolds number on the centre-line of the plane layer being over 400 at $s = 30$ cm. Evidently the existence of universal equilibrium in intermittently turbulent flow deserves further study.

We have given some thought to the best way of presenting the data for the curved shear layer, and finally chose contour plots in s, n/δ axes, where s is the distance from the nozzle lip measured along an arbitrarily chosen curved centre-line (not a streamline), n is the distance measured normal to the centre-line and towards the centre of curvature, at any given s, and δ is the thickness of the shear layer: for definitions and data see figures 1–3 and § 3, and for a general review of

co-ordinate systems and equations for curved flows see Bradshaw (1973). The graphs show these contours mapped on to rectangular x, n/δ axes. The derivative following a mean streamline in real space is most simply obtained from the following expression, valid for small $d\delta/ds$:

$$\frac{D}{Dt} = \frac{U}{(1+n/R)}\left[\frac{\partial}{\partial s} + \left\{\left(\frac{d(n/\delta)}{ds}\right)_{\psi} + \frac{n}{\delta}\frac{1}{\delta}\frac{d\delta}{ds}\right\}\frac{\partial}{\partial n/\delta}\right], \tag{1}$$

where all distances are measured on the rectangular graphs. Here U is the s component of the velocity, R is the (variable) radius of curvature of the s axis, which is *negative* by convention in this flow, and $(d(n/\delta)/ds)_{\psi}$ is the local inclination of the mean streamline to the s axis of the rectangular graph. $d\delta/ds$ and $1/R$ are plotted against s in figure 2. Note that the axes and notation used in this paper differ in detail from those used by Castro (1973).

3. Results

Figure 1 shows the path of the shear layer, the edges being shown as wavy lines. For quantitative purposes the thickness δ was chosen as the distance between the points where $(P-p_a)/\frac{1}{2}\rho U_{\text{ref}}^2$ took values of 0·81 and 0·0625; here P is the total pressure measured with a Pitot tube and p_a is the atmospheric pressure. In a plane mixing layer with a static pressure negligibly different from atmospheric these definitions give the points $U/U_{\text{ref}} = 0{\cdot}9$, $0{\cdot}25$, whose distance apart is $0{\cdot}113x$. We deliberately chose points not too far from the centre of the shear layer so that the thickness δ, used as a length scale, should not be affected by minor eccentricities near the extreme edges of the profiles. The 'centre-line' is $0{\cdot}39\delta$ from the high velocity 'edge' and would coincide with the true centre-line, where $P-p_a \simeq 0{\cdot}45 \times \frac{1}{2}\rho U_{\text{ref}}^2$, in a plane mixing layer. These definitions are of course arbitrary and are used only in mapping the mixing layer into a rectangle for ease of presentation of results. The region of large curvature extends between about 15 and 50 cm from the nozzle lip, and in this region the centre of curvature of the centre-line is near the point $x = 12{\cdot}6$ cm, $y = 25{\cdot}1$ cm with respect to the nozzle lip. This point, P in figure 1, was chosen as the origin of radial traverses and of polar co-ordinates (r, θ), and the shear-layer geometry is most easily recovered from the plots of r, $\phi \equiv -\tan^{-1}(dr/ds)$, s and δ against θ in figure 2(*a*): the total angle through which the centre-line has been deflected is $\theta+\phi$. The centre-line curvature $\kappa \equiv 1/R$ and the growth rate $d\delta/ds$ are plotted against s in figures 2(*b*) and (*c*). Beyond $\theta = 90°$ polar co-ordinates are not used because the layer rapidly becomes straight, and the centre-line coincides with the line $x = 35{\cdot}4$ cm, 9·3 cm from the backplate. In this region $d\delta/ds$ also becomes sensibly constant, but at a value some 9% higher than that in a plane layer: the Reynolds stresses are not exactly self-preserving, and eventual relaxation to the plane-layer state is expected.

The polar co-ordinates of the 'reference' streamline, which leaves the nozzle at $y = -4$ cm and asymptotes to $x \simeq 40$ cm near the backplate before finally entering the shear layer, are given in figure 3 as plots of r, ϕ and s against θ,

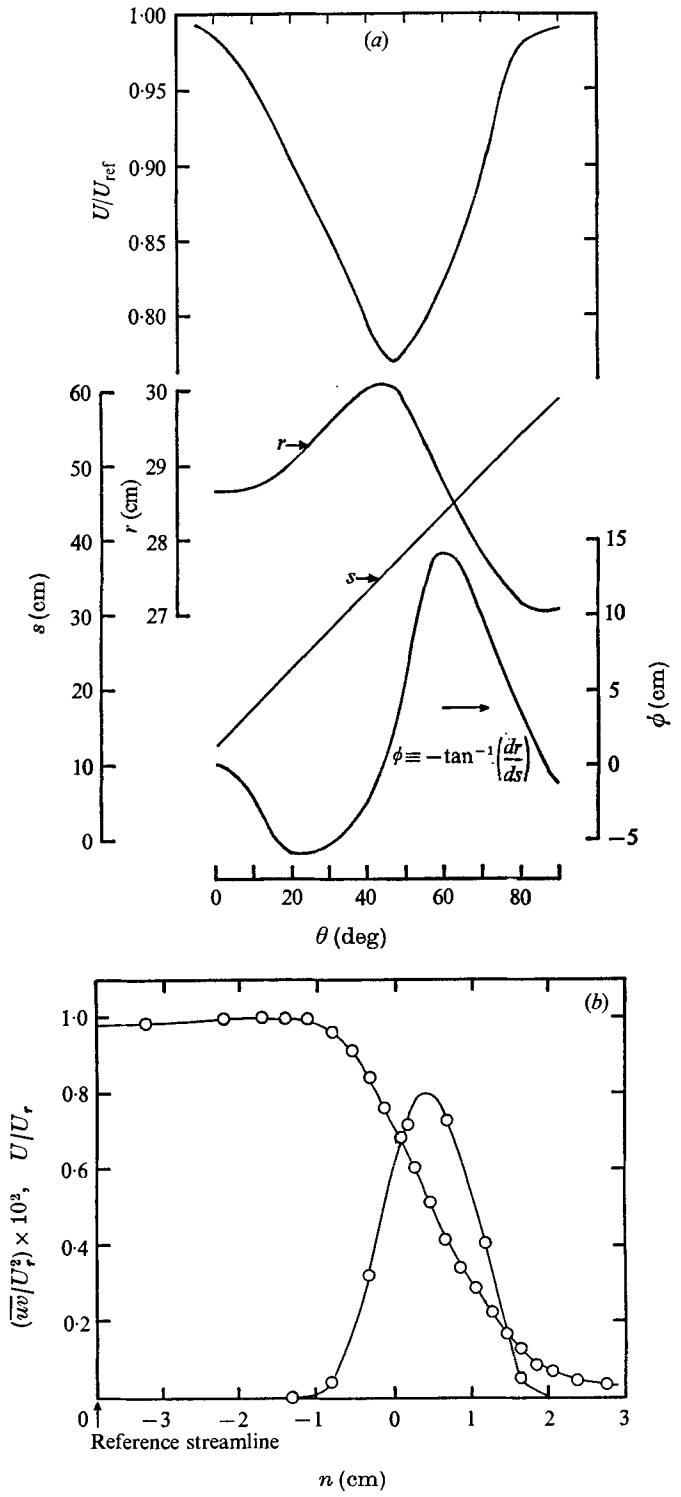

FIGURE 3. Boundary conditions. (*a*) Conditions on reference streamline. (*b*) Velocity and shear-stress profiles at $s = 12{\cdot}6$ cm, $\theta = 0$; $\delta = 1{\cdot}51$ cm, $r_{\mathrm{ref}} = 24{\cdot}8$ cm.

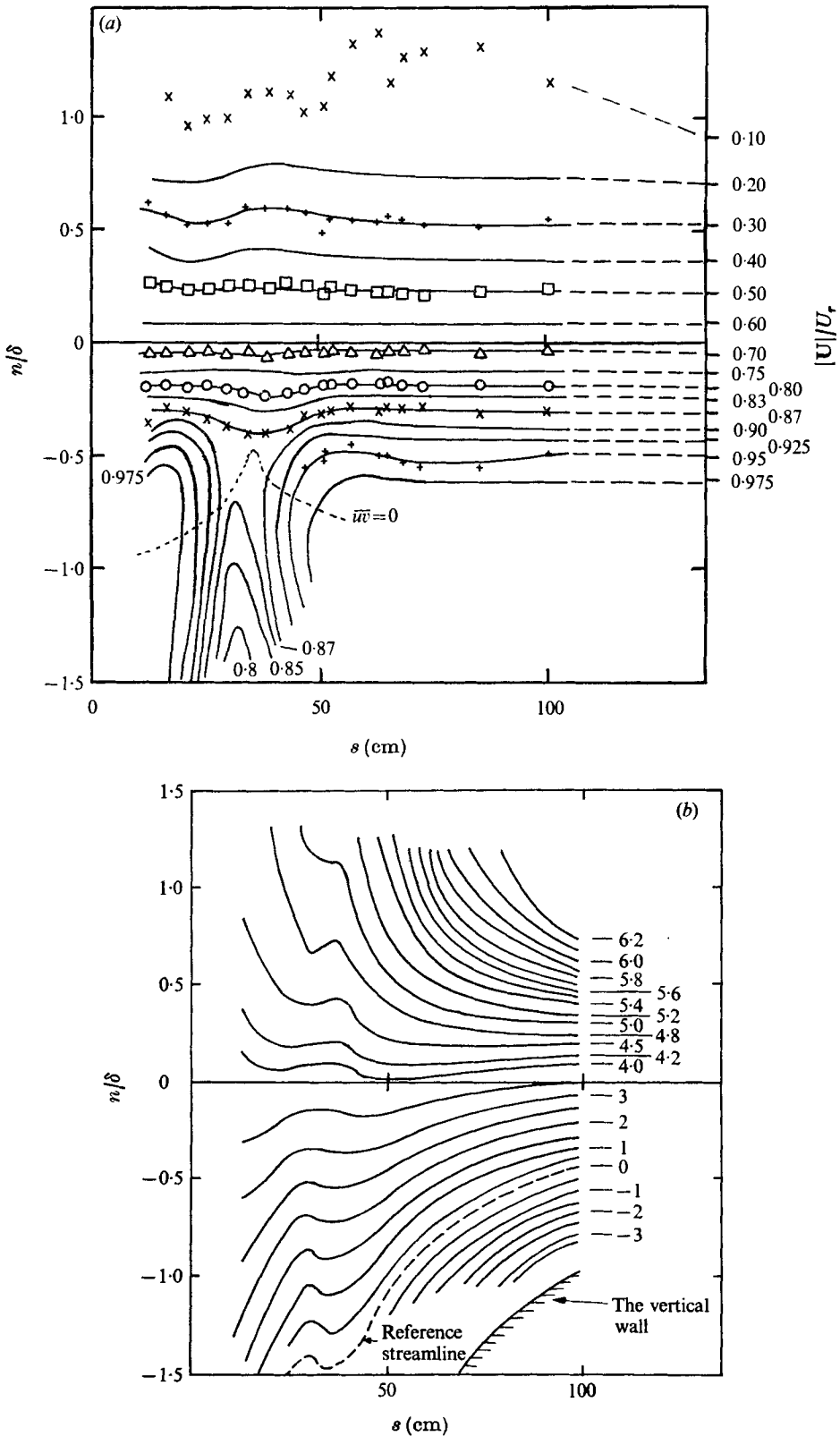

FIGURES 4(*a*, *b*). For legend see page 281.

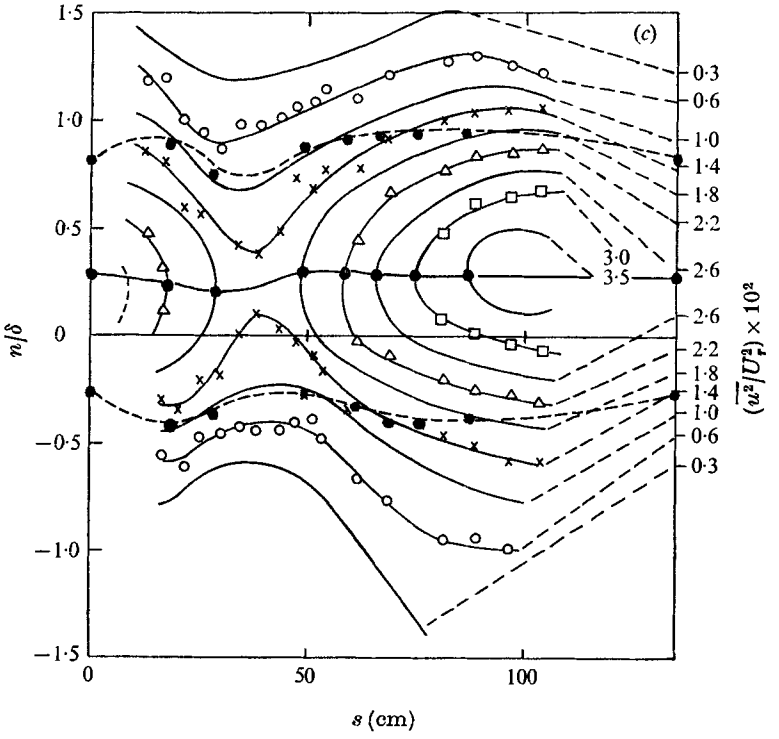

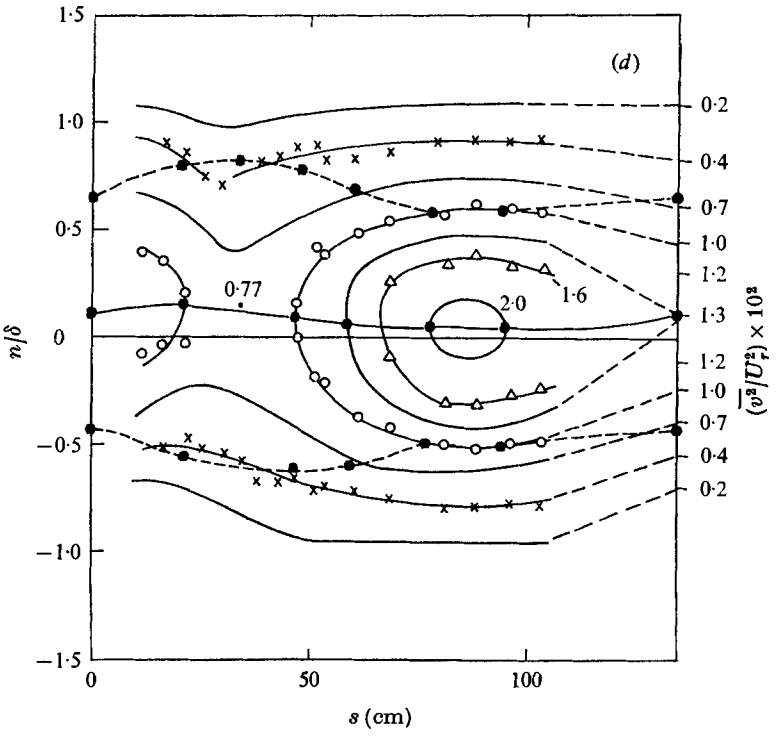

FIGURES 4(*c*, *d*). For legend see page 281.

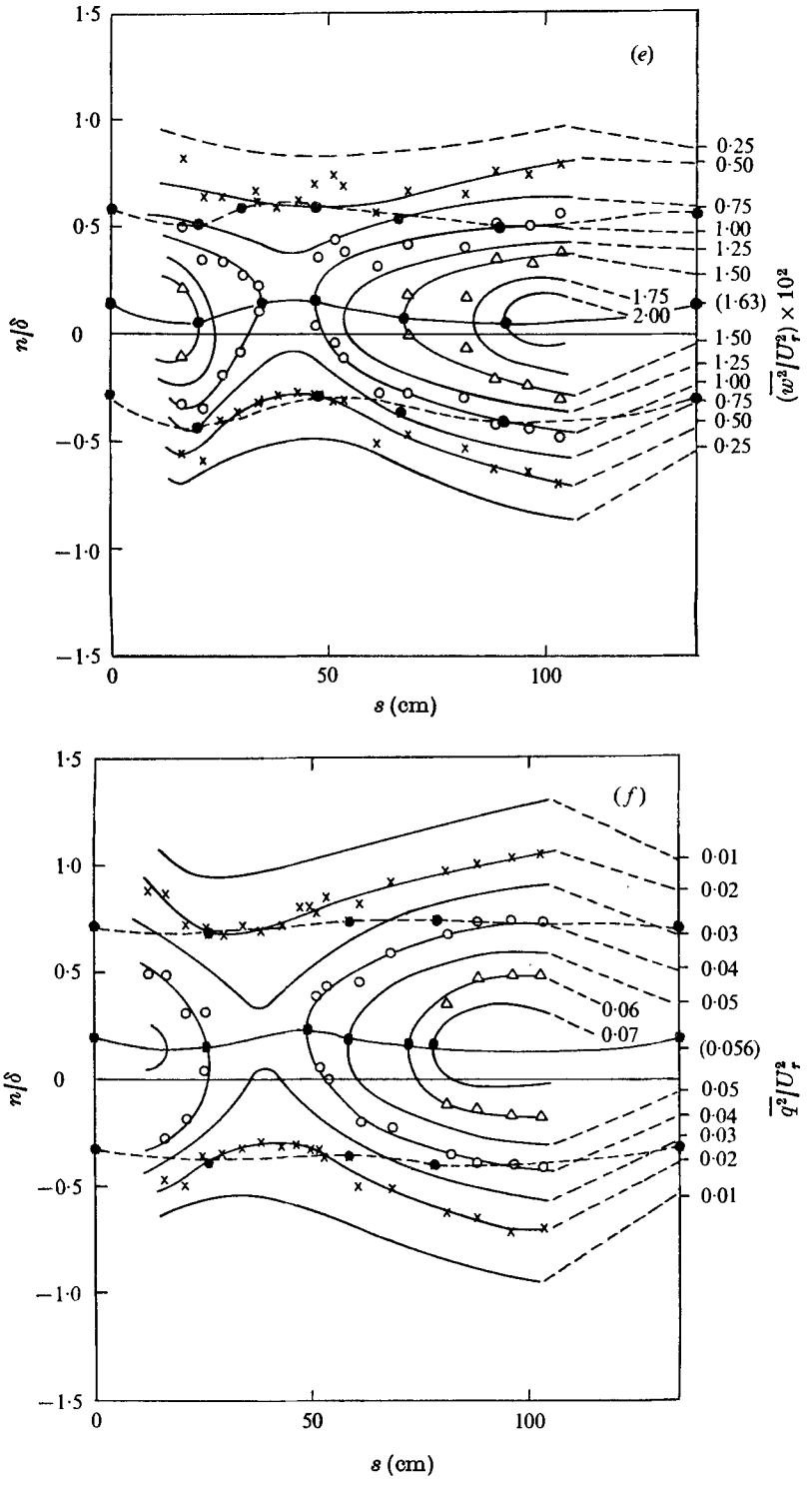

FIGURES 4(*e*, *f*). For legend see page 281.

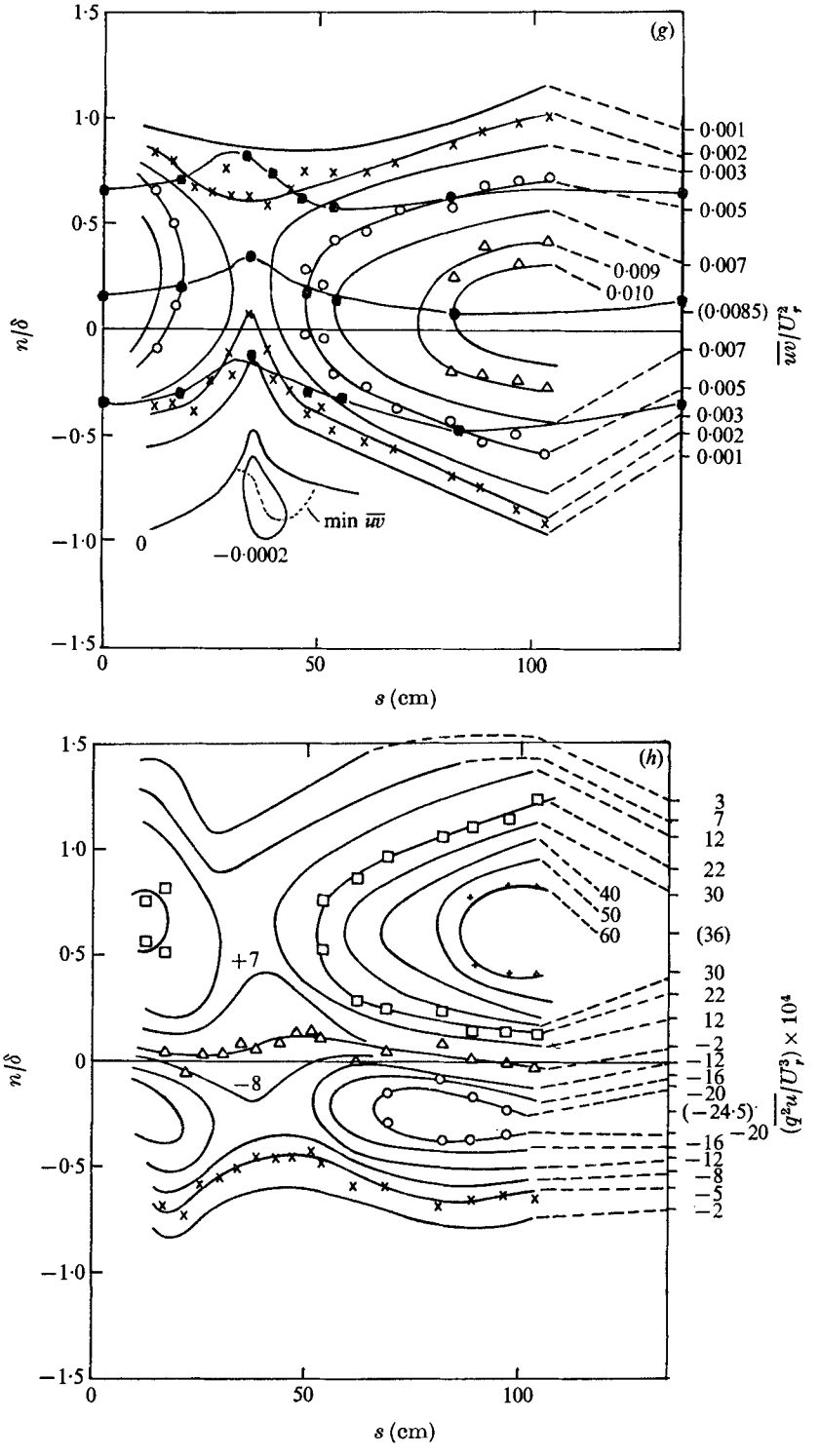

FIGURES 4(*g*, *h*). For legend see page 281.

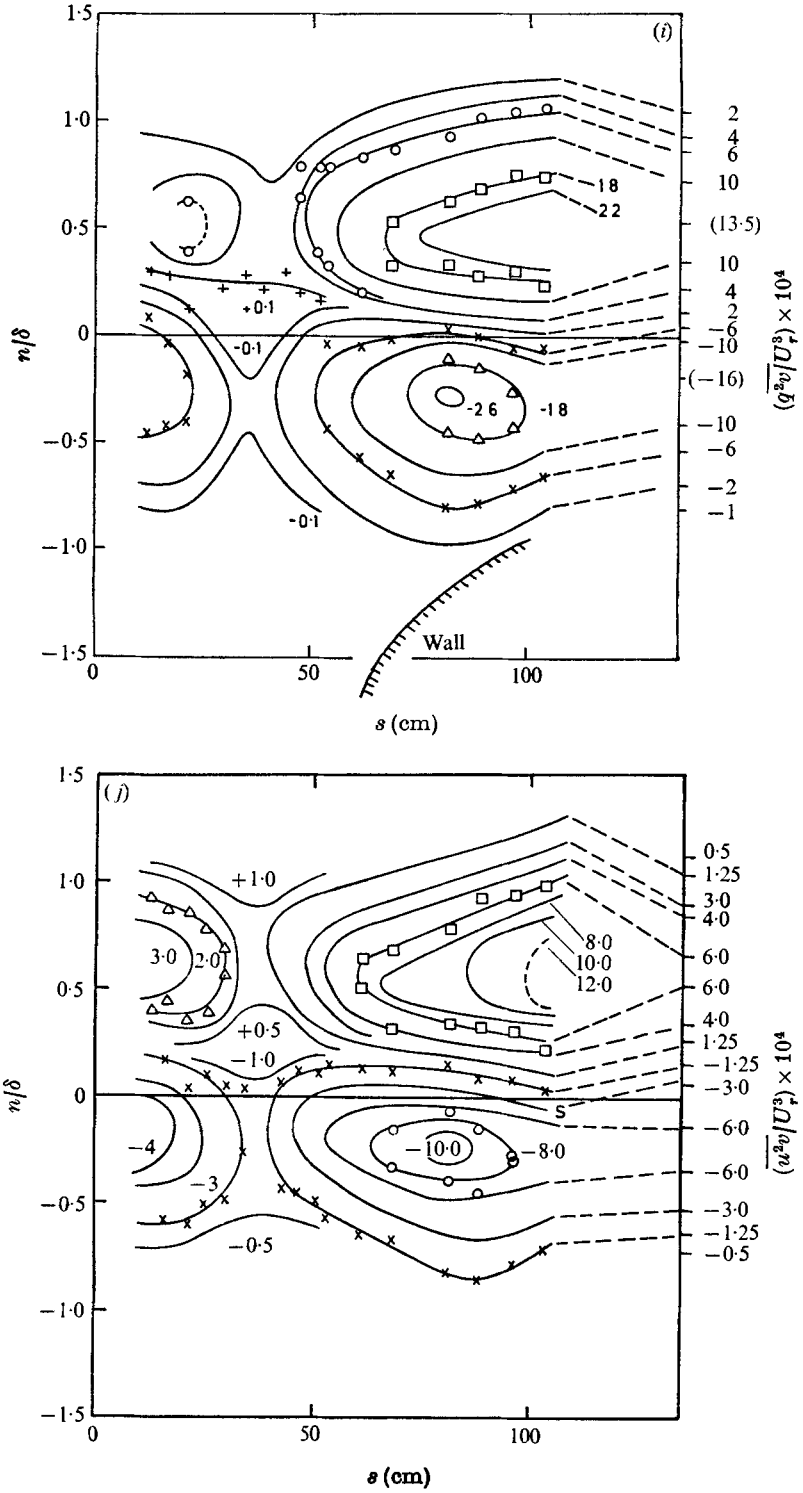

FIGURES 4(*i*, *j*). For legend see page 281.

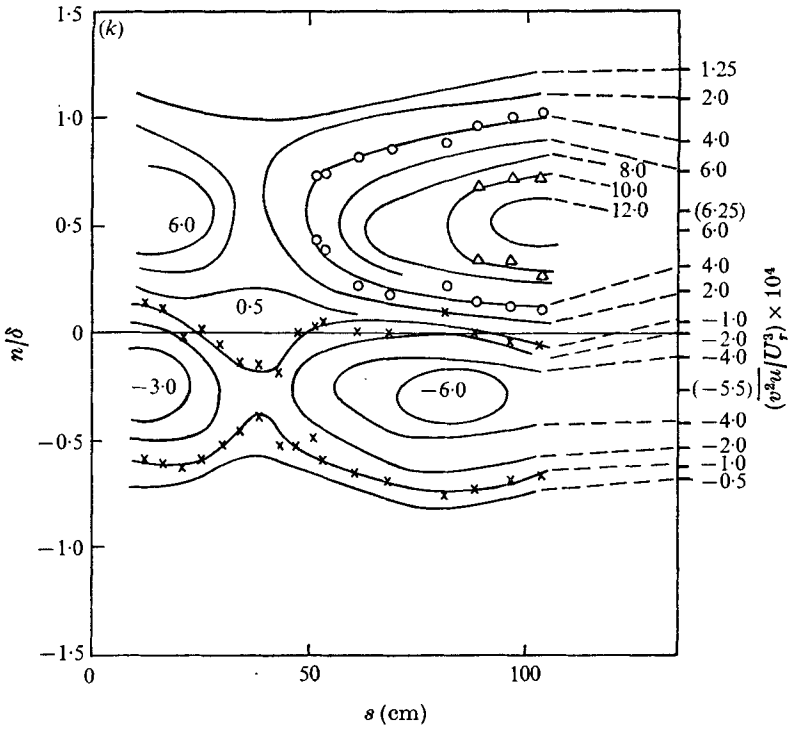

FIGURE 4. Contours in s, n/δ co-ordinates, mapped onto a rectangle: figures at right are plane-layer values at same n/δ. Points (cross-plotted from profiles) show typical scatter and identify disconnected contours. (*a*) Resultant mean velocity (closely equal to U for $n/\delta < 1{\cdot}0$). (*b*) Stream function $\psi \equiv \int U\,dn/U_{\text{ref}}$ (cm), origin on reference streamline: nozzle separation streamline is $\psi = 4$ approximately. (*c*) s-component mean-square intensity. (*d*) n-component mean-square intensity. (*e*) Spanwise-component mean-square intensity. (*f*) Resultant mean-square intensity $\overline{q^2} \equiv \overline{u^2}+\overline{v^2}+\overline{w^2}$ ($2 \times$ turbulent energy). (*g*) Shear stress in s, n co-ordinates. (*h*) Triple product $\overline{q^2u}$. (*i*) Triple product $\overline{q^2v}$. (*j*) Triple product $\overline{u^2v}$. (*k*) Triple product $\overline{uv^2}$.

together with the velocity along the streamline. The proper boundary conditions for a complete calculation of the flow are the magnitude and direction of the mean velocity on the reference streamline (figure 3*a*), the profiles of mean velocity (figure 3*b*) and any other required quantities at the first measurement station, $s = 12{\cdot}6$ cm, together with the profiles at the *last* measurement station and a suitable approximation to zero velocity at 'infinity' to complete the boundary conditions for an elliptic solution.

The main results are plotted as contours in s, n/δ co-ordinates in figures 4(*a*)–(*k*). The results of the companion experiment in a plane self-preserving mixing layer are shown at the right-hand side of each figure (except figure 4*b*) as the notional asymptotes for large (and small) s, though in practice the flow at small s is affected by transition of the laminar nozzle boundary layer while at large s the mixing layer spreads to the backplate. Values in parentheses are the extremum values in the plane layer.

The velocities shown in figures 4(*a*)–(*k*) are resolved along and normal to the local centre-line (that is, the axes do not vary with n). This choice, like that of the co-ordinate mapping, was made so that departures of the results from plane-mixing-layer behaviour could be attributed to changes in turbulence structure and not to geometry *per se*. The quantities plotted have all been measured directly except for $\overline{q^2u} \equiv \overline{u^3} + \overline{uv^2} + \overline{uw^2}$ and $\overline{q^2v} \equiv \overline{u^2v} + \overline{v^3} + \overline{vw^2}$: in the latter cases the terms containing w were not measured in full but were assumed to bear the same ratio to the complete triple product as in the plane mixing layer, on the basis of a few check measurements. The streamlines in figure 4(*b*) show the entrainment flow into the shear layer: the complete entrainment flow rate on the low velocity side up to $s = 100\,\text{cm}$, which must be simulated roughly in elliptic calculations as a flow across the boundary at 'infinity', is about $3U_{\text{ref}}$ cm^3s^{-1} per unit span.

Plots of derived quantities are introduced in the discussion below.

4. The 'fairly thin shear layer' approximation

As shown in the introduction, most flows with significant Reynolds-stress gradients are fairly thin shear layers, having $d\delta/dx$ and $e(\partial U/\partial y)^{-1}$ fairly small compared with unity. Qualitatively, this permits us to regard such flows as perturbations of classical shear layers such as the plane mixing layer, but the shear-layer concept is of quantitative use only if it permits simplifications of the equations of motion. The thin-shear-layer (or 'boundary layer') approximation permits the *neglect* of some terms in the equations if $d\delta/dx$ is *very* small compared with unity. If $d\delta/dx$ and $e(\partial U/\partial y)^{-1}$ are *fairly* small we can expect that the terms which are neglected in the corresponding thin shear layer will be small enough to be *approximated*. This 'fairly thin shear layer' (FTSL) approximation is necessarily less rigorous than the classical thin-shear-layer approximation but it is the only possible bridge between thin shear layers and flows requiring the full Navier–Stokes equations. Clearly the concept applies to laminar or turbulent flows: in practice the main applications are to the treatment of turbulent flows with empirical Reynolds-stress models which are already approximate. The concept of approximating, rather than neglecting, terms is not new, even in the present context, but its application to shear layers has been fragmentary. This is a convenient opportunity to clarify the concept, and to test it in a flow in which its use is virtually essential if the results are to be related to existing data for classical shear layers.

We are entitled to choose curvilinear co-ordinate axes so as to make the terms which we need to approximate as small as possible, and a prerequisite of the use of the FTSL approximation is to define the direction of the shear layer, which, as in a thin shear layer, will be chosen as the longitudinal axis. There is no need for a general definition since one object of the approximation is to relate the actual flow to a particular species of classical thin shear layer, whose properties can be invoked in the definition: however one's confidence in the approximation as a concept would be increased if, in the present highly curved flow, the various plausible definitions of shear-layer direction were to coincide.

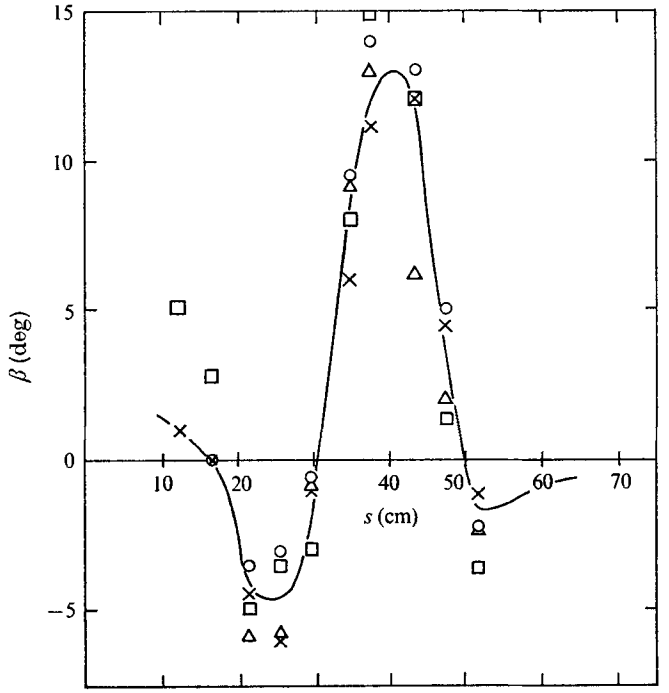

FIGURE 5. Comparison of definitions of shear-layer direction. ×, β_1; ○, β_2; △, β_3; □, β_4. See § 4 for notation.

Some possible definitions are the following.

(i) The direction β_1 of the 'centre-line' defined at the beginning of § 3: this direction happens to coincide, within the accuracy of measurement, with the line on which the mean velocity is 0·67 of the reference velocity, as it does in a plane mixing layer.

(ii) The direction β_2 of the locus of points of maximum turbulent energy minus 0·017 rad (1°); $\overline{q^2}$ is a maximum at $y/x = 0{\cdot}017$ in a plane mixing layer.

(iii) The direction β_3 of the mean streamline at $U/U_{\text{ref}} = 0{\cdot}67$ minus 0·01 rad (0·6°): V/U is about 0·01 at $y = 0$ in a plane mixing layer.

(iv) The direction β_4 of the line having the same inclination to the expansive rate of strain at $U/U_{\text{ref}} = 0{\cdot}67$ as does the $y = 0$ line in a plane mixing layer.

The four definitions are plotted in figure 5, angles being measured (figure 1) with respect to a constant-r line: β_1 is of course the same as ϕ, plotted against θ in figure 2(a). Except at the first measuring point the different definitions are seen to coincide within the likely experimental accuracy (streamline angles measured with a cross-wire probe generally agreed to within about 1° with those deduced from resultant velocity measurements using the continuity equation). In fact a small consistent difference between (i) and (ii) can be seen from the contour plots of turbulent intensity (in which the definition (i) is used for the s axis). We have *not* tried any more refined definitions based on the behaviour of the

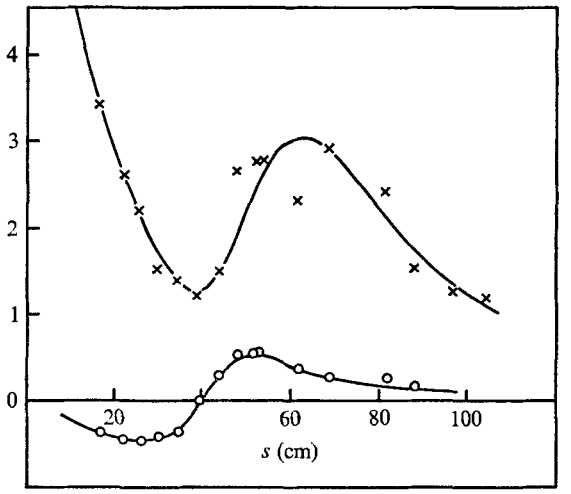

FIGURE 6. Reynolds-stress gradients in the streamwise momentum equation. ×, $[(\partial(\overline{uv})/\partial n)U_r^{-2}] \times 10^3$ (cm^{-1}) (maximum values); ○, $[(\partial\overline{u^2}/\partial s)\,U_r^{-2}] \times 10^3$ (cm^{-1}) (centre-line values).

Reynolds-stress tensor because, as mentioned in the introduction, it appears to be the first law of complex flows that this behaviour will differ significantly from that in a shear layer unaffected by extra rates of strain.

The most obvious use of the FTSL concept is in approximating the normal-stress gradient terms in the equations of motion referred to axes along and normal to the direction of the shear layer. These terms are *neglected* in the thin-shear-layer equations. Figure 6 shows the normal-stress gradient $\partial\overline{u^2}/\partial s$ in the s-component momentum equation compared with the shear-stress gradient $\partial\overline{uv}/\partial n$: the most relevant comparison seems to be between the maximum $\partial\overline{u^2}/\partial s$, which occurs near the centre-line (where it would be zero in a plane mixing layer), and the maximum $\partial\overline{uv}/\partial n$. Now, using x, y co-ordinates along and normal to the local streamline, the streamwise momentum equation can be written in terms of the total pressure P as

$$\frac{\partial}{\partial x}\left(\frac{P}{\rho}+\frac{\overline{u^2}}{2}\right) = \frac{-\partial\overline{uv}}{\partial y}. \tag{2}$$

Therefore, although large negative values of $\partial\overline{u^2}/\partial s$ occur, followed by large positive values as the flow recovers, the net effect on the total pressure on a given streamline is small enough for a crude approximation to $\partial\overline{u^2}/\partial s$ to suffice in a calculation method. It seems that this will be true in fairly thin shear layers in general: large and permanent changes in $\overline{u^2}$ occur only in flows whose mean velocity is changed by a large and permanent amount by strong longitudinal pressure gradients, which dominate the normal-stress terms anyway. Note that in s, n co-ordinates a term $2\overline{uv}/R$ appears in the s-component momentum equation (see, for example, Bradshaw 1973), where R is the radius of curvature of the s axis: clearly this term can be retained in 'exact' form since $\overline{uv}$ will always be evaluated explicitly in a calculation method.

These considerations suggest that discussion of the present results in the context of the 'fairly thin shear layer' approximation and with reference to measurements in a plane mixing layer will be meaningful. The alternative would be to ignore any preferred directions and discuss the magnitude and direction of the principal stresses and strain rates (or the stresses and strain rates referred to arbitrary fixed axes, which would be even less helpful): a brief discussion is given by Castro (1973). In calculation methods, any explicit dependence of empirical input or approximation on preferred directions leads to model equations which are not rotationally invariant, and this gives pain to some people. This is not the place for a full discussion; readers with doubts can simply regard the s, n axes as a pragmatic extension of the axes used in the thin-shear-layer equations (themselves non-invariant), chosen to reveal and correlate differences between the curved flow and a plane mixing layer.

As pointed out by Bradshaw (1973, §5.1), most of the parameters which are commonly used to describe curvature effects can be related to the rate-of-strain ratio $e\,(\partial U/\partial y)^{-1} = (\partial V/\partial x)\,(\partial U/\partial y)^{-1} = -(U/r)\,(\partial U/\partial n)^{-1}$, where r is the local radius of curvature of the mean streamline. A parameter with a direct physical interpretation (Wyngaard 1967) is

$$R_f = \frac{2U/r}{\partial U/\partial n + U/r}, \tag{3}$$

which is (minus) the ratio of the v-component energy production term (due to streamline curvature) to the u-component energy production term. This verbal definition is the same as that of the flux Richardson number for buoyant flows. $\partial U/\partial n$ can be thought of as a typical angular velocity of the basic shear: a typical angular velocity of the energy-containing turbulence, say $(\overline{uv})^{\frac{1}{2}}/L$, might be thought more realistic, but if the flow is in local energy equilibrium the two are directly related and equal to a first approximation. The present flow is not in local equilibrium but the behaviour of $\overline{uv}$ and L is so unusual that we have retained $\partial U/\partial n$ as a typical frequency, and use R_f as a curvature parameter.

5. Effects of streamline curvature on the turbulence

The turbulent energy equation and the shear-stress transport equation in s, n co-ordinates are, omitting the viscous diffusion term in the former equation and the complete viscous terms in the latter as is customary at high Reynolds numbers,

$$\begin{aligned}\left(1+\frac{n}{R}\right)\frac{D}{Dt}(\tfrac{1}{2}\overline{q^2}) &\equiv \underline{\left[U\frac{\partial}{\partial s}+\left(1+\frac{n}{R}\right)V\frac{\partial}{\partial n}\right](\tfrac{1}{2}\overline{q^2})}\\ &= -\overline{u^2}\left[\frac{\partial U}{\partial s}+\frac{V}{R}\right]-\left[1+\frac{n}{R}\right]\overline{v^2}\frac{\partial V}{\partial n}-\overline{uv}\underline{\left[\left(1+\frac{n}{R}\right)\frac{\partial U}{\partial n}-\frac{U}{R}+\frac{\partial V}{\partial s}\right]}\\ &\quad -\frac{\partial}{\partial s}\left(\overline{\frac{p'u}{\rho}}+\tfrac{1}{2}\overline{q^2u}\right)-\underline{\frac{\partial}{\partial n}\left[\left(1+\frac{n}{R}\right)\left(\overline{\frac{p'v}{\rho}}+\tfrac{1}{2}\overline{q^2v}\right)\right]}\\ &\quad -\epsilon,\end{aligned} \tag{4}$$

where the four lines on the right represent respectively the mean transport

(advection), production, turbulent transport (diffusion) and dissipation, the leading terms being underlined, and

$$\left(1+\frac{n}{R}\right)\frac{D}{Dt}(-\overline{uv}) \equiv \underline{\left[U\frac{\partial}{\partial s}+\left(1+\frac{n}{R}\right)V\frac{\partial}{\partial n}\right](-\overline{uv})}$$
$$= \overline{u^2}\left(\frac{\partial V}{\partial s}-\frac{U}{R}\right)+\underline{\left(1+\frac{n}{R}\right)\overline{v^2}\frac{\partial u}{\partial n}}-(\overline{u^2}-\overline{v^2})\frac{U}{R}$$
$$\underline{-\frac{\overline{p'}}{\rho}\left[\frac{\partial V}{\partial s}+\left(1+\frac{n}{R}\right)\frac{\partial U}{\partial n}\right]}$$
$$+\frac{\partial}{\partial s}\left(\frac{\overline{p'v}}{\rho}+\overline{u^2v}\right)+\underline{\left(1+\frac{n}{R}\right)\frac{\partial}{\partial n}\left(\frac{\overline{p'u}}{\rho}+\overline{uv^2}\right)}+\frac{2\overline{uv^2}-\overline{u^3}}{R}, \quad (5)$$

where the four lines on the right represent respectively the mean transport, generation, pressure–strain redistribution and turbulent transport. In the present case, n is taken positive towards the centre of curvature for conformity with the x, y axes used in plane mixing layers and R and its reciprocal κ are negative. The parts of the generation terms in each equation that involve R therefore reduce the magnitudes of the total terms, so that a 'stabilizing' effect of curvature is expected though its magnitude cannot be judged from the behaviour of the generation terms alone. It is important to note that, at any rate in the present flow, the term $(\overline{u^2}-\overline{v^2})\,U/R$ in the shear-stress equation, representing the change in shear stress due to rotation of the axes, is rather small. The change in $\overline{uv}$ caused by rotating the axes through an angle θ in the s, n plane is

$$-2\overline{uv}\sin^2\theta-(\overline{u^2}-\overline{v^2})\sin\theta\cos\theta$$

and so only the second term produces first-order effects for small θ. (For large angles both terms become large but in real flows large changes in direction cannot usually be enforced quickly, so that this analysis is not relevant.) In the present flow the rotation term is quite small until $\overline{uv}$ has already fallen by a large amount. Also, rotation of the axes cannot be blamed in any indirect way for the behaviour of $\overline{uv}$. The angle between the larger principal stress and the principal rate of strain is roughly constant round the s axis (Castro 1973).

The effects of curvature on the shear stress and intensity are large: the maximum value of the resultant intensity $\overline{q^2} \equiv \overline{u^2}+\overline{v^2}+\overline{w^2}$ at a given station (figure 7*a*) falls, nominally from the self-preserving value of $0{\cdot}056U_{\rm ref}^2$, to $0{\cdot}03U_{\rm ref}^2$ at $s = 40$ cm, and $\overline{uv}/U_{\rm ref}^2$ falls from 0·0085 to 0·0025. Large decreases in turbulent activity in the stably curved region were expected; it was *not*, however, expected that the shear stress and intensity would overshoot the plane-layer values by factors of about 1·3 before finally asymptoting to the latter. This appears to be a new aspect of the behaviour of turbulence: the only known phenomenon likely to be related to it is the overshoot in turbulence intensity in the later stages of transition. Very recently Young (unpublished work at Imperial College) has found a similar overshoot in a boundary layer downstream of a 30° convex (stable) bend with a radius of curvature about five times the boundary-layer thickness, so the phenomenon is likely to be a general response to a short region of large stabilizing strain rate rather than a peculiarity of the present configuration or of the mixing layer alone.

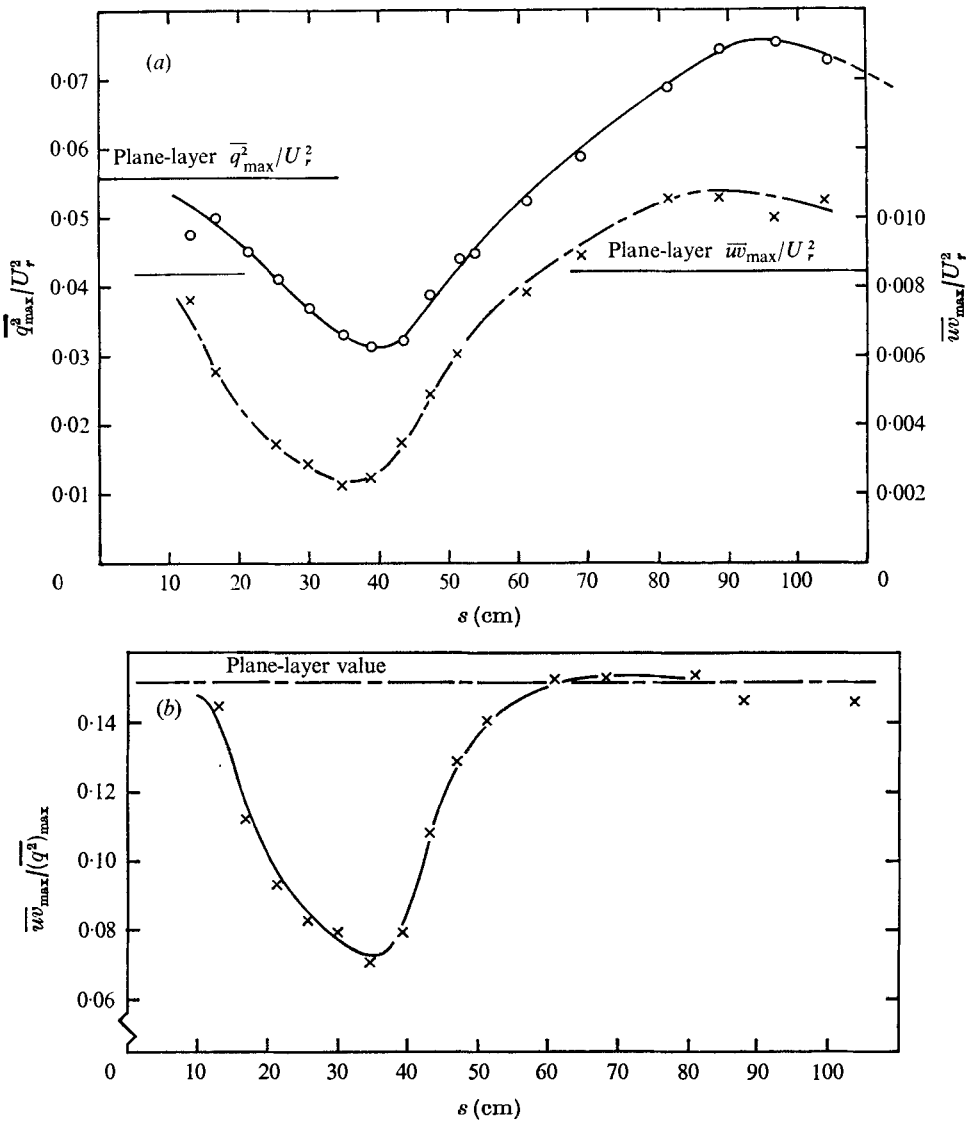

FIGURE 7. Streamwise variation of turbulent energy and shear stress. (*a*) Maximum turbulent energy (circles) and shear stress (crosses). (*b*) Structure parameter $\overline{uv}/\overline{q^2} \equiv a_1$ on centreline.

The variations in the n direction (the 'profiles') of the turbulence quantities shown in figures 4(*c*)–(*k*) are generally unremarkable. The dashed lines on the contour plots of the intensities and shear stress join the points where the plotted quantity is half the maximum value on the profile, so that the distance between the lines is a simple measure of the profile shape (a small distance means a peaky profile and vice versa). In the case of $\overline{q^2}$ the lines are very nearly straight and parallel to the axis, but of the individual intensity profiles $\overline{u^2}$ becomes significantly more peaky, and $\overline{v^2}$ less peaky, in the region of maximum streamline curva-

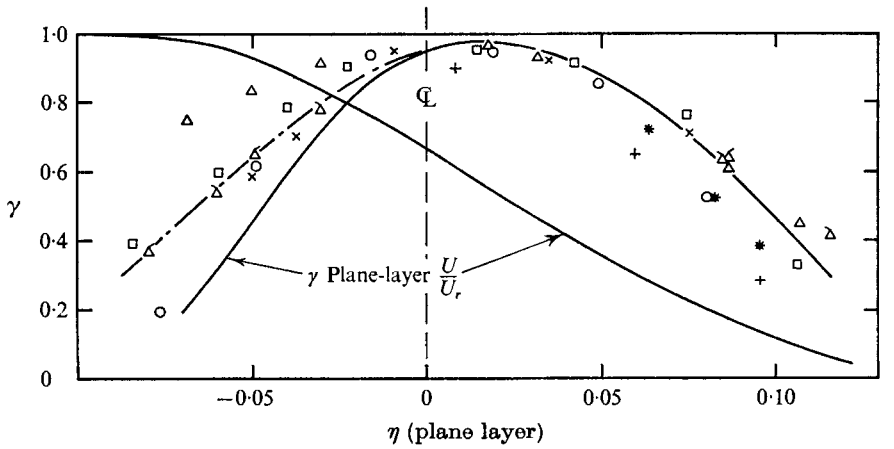

FIGURE 8. Intermittency factor, referred to plane layer at positions of same total pressure. ×, s = 21·1 cm; ○, 29·9; □, 34·4; △, 38·8 (from u-component flatness factor); +, s = 81·5; *, s = 81·5 (flatness factor).

ture near s = 30 cm. The peakiness of the $\overline{uv}$ profile does not change significantly but the point of maximum shear stress moves out rather sharply towards the low velocity side of the layer near s = 30 cm. The positions of the maxima of the other profiles wander about slightly but consistently with respect to the arbitrary centre-line: the effect would be reduced by adopting definition (ii) of § 4 for the centre-line, instead of definition (i). The shift of $\overline{uv}$ with respect to the other profiles does seem to be significant (profiles were measured at s intervals of 4·4 cm in this region so the deductions do not rely on one traverse only). Possibly the stress tensor in the slow-moving fluid near the low velocity side of the layer can rotate more rapidly, in terms of s, so that $\overline{uv}$ is less influenced by the axis-rotation effects discussed above (most other plausible explanations would predict a shift in $\overline{q^2}$ as well as $\overline{uv}$). There is a small region of negative $\overline{uv}$ on the high velocity side of the layer near s = 30 cm caused by the change in sign of $\partial U/\partial n$ in this region: in the free stream the moment of momentum is constant, so that U decreases with increasing distance from the centre of curvature, and in the region of maximum curvature this decrease begins well inside the shear layer. The shear stress $\overline{uv}$ seems to react more quickly than the turbulent intensity but the effect on $\overline{uv}$ is more eye-catching because it can change sign whereas the intensity cannot.

The triple products (figures 4*h–k*) change sign near the centre-line, all those shown being positive for positive n (approximately) and conversely. The contours of zero triple product (not necessarily shown in the figures) move towards the high velocity side of the layer after the region of strong curvature, and while the maximum values ($n > 0$) continue to grow the minimum values ($n < 0$) are greatest near s = 80 and then decline rather sharply. The movement of the zero contour is probably real but the sharp decline on the high velocity side is at least partly attributable to the presence of the wall. The wall (or the mirror-image flow which can be regarded as replacing it) sets up pressure fluctuations to

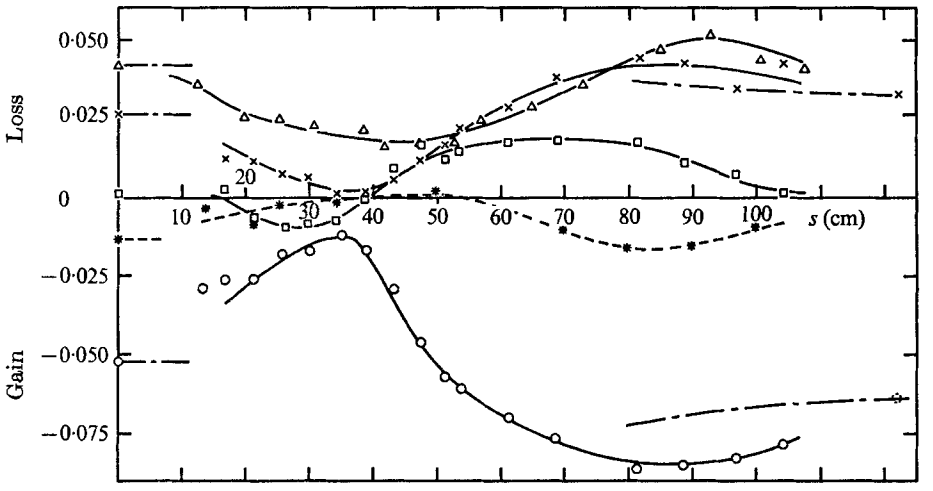

FIGURE 9. Terms in turbulent energy equation on centre-line: all quantities made dimensionless by U^3_{ref}/s. □, advection; ○, production; ×, diffusion; △, dissipation; – – –, out-of-balance term; ——·——, plane-layer values.

reduce the normal-component velocity to zero at the wall, and thus inhibits the turbulent motion, particularly that of the larger eddies. It is noticeable that $\overline{q^2v}$ falls more sharply than $\overline{q^2u}$, as would be expected from this explanation. This phenomenon, which has nothing to do with shear-layer curvature, deserves further study: it is a nice demonstration of the effect of a solid surface on turbulence in general and the pressure-fluctuation field in particular, and of the dominance of large eddies in triple-product transport.

The intermittency factor γ has not been fully explored, because the sample profiles shown in figure 8 showed that, when plotted against the total pressure (which appeared to be the best basis for comparisons), γ is little affected by curvature. Indeed the main effect of curvature seems to be on the algorithm used to determine γ from digitized fluctuation signals, which gave peculiar results near the high velocity edge in the region of maximum curvature. Examination of oscilloscope traces in this region showed that the irrotational motion was very strong: the intermittency at $s = 38{\cdot}8$ cm, denoted by flagged triangles in figure 8, was obtained by manual measurement from chart recordings of the oscilloscope traces. All the indications are that these strong irrotaticnal fluctuations are due to wave motion in the highly stabilized region, similar to that shown in the shadowgraphs of Pao (1969) in a stably stratified flow, but as yet no two-point measurements have been made to investigate the propagation velocity in the irrotational region.

If it is accepted that the changes in profile shape are of secondary importance to the general streamwise trend of a reduction in turbulent activity in the highly curved region followed by overshoot and relaxation, the flow phenomena can be discussed mainly in terms of properties on the centre-line, where the second-order products are virtually at their maximum values. The maximum intensity and shear stress, and their ratio ($\simeq \overline{uv}/q^2$) on the centre-line, are plotted against s

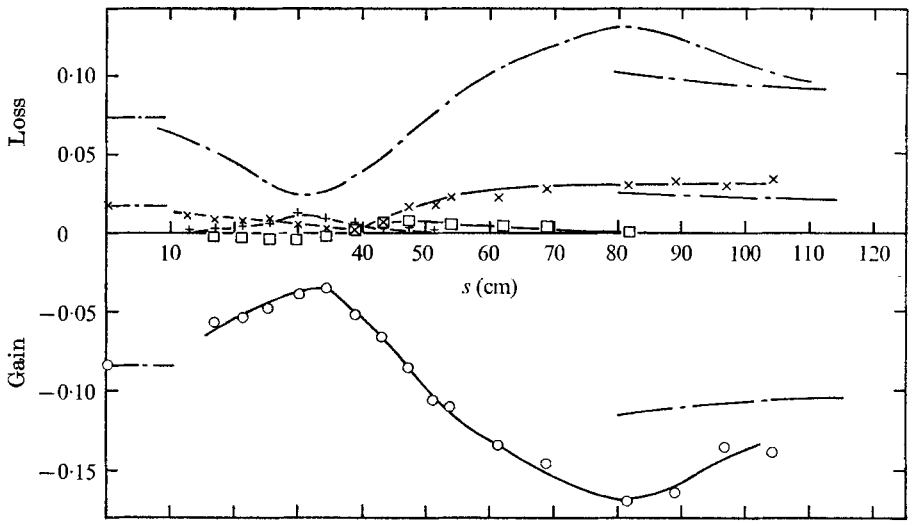

FIGURE 10. Terms in $\overline{uv}$ transport equation (referred to s, n co-ordinates) on centre-line: all quantities made dimensionless by $U_{\text{ref}}^3/\text{s}$. □, mean transport; ○, generation; ×, turbulent transport; +, rotation $-U(\overline{u^2}-\overline{v^2})/R$; – – – –, pressure–strain 'redistribution', by difference; —·—·—, plane-layer values.

in figures 7(*a*) and (*b*). The terms in the turbulent energy equation and the $\overline{uv}$ transport equation on the centre-line are plotted against s in figures 9 and 10, made dimensionless by $U_{\text{ref}}^3/\text{s}$; note that the thin-shear-layer approximation has not been used. Turbulent transport by pressure fluctuations has been neglected in both cases, and the main destruction term in the $\overline{uv}$ transport equation, the pressure–strain 'redistribution' term, has been obtained by difference. The neglect of pressure transport can be checked near the edges of the shear layer, where we expect that (transport by mean flow) = (transport by turbulence) and the difference between mean transport and the measured triple-product turbulent transport appears as an 'out-of-balance' term, and neglect is justified in the plane layer (figures 11*a* and 12*a*). In the curved layer (figures 11*b–d*) pressure transport of turbulent energy near the high velocity edge is significant in the highly curved region, where the irrotational fluctuations (possible waves) are large, and also far downstream, where the shear layer has nearly reached the backplate. This is compatible with the suggested presence of wave motion in the one case and the influence of the solid surface on the large eddies in the other. It is more difficult to draw conclusions from the $\overline{uv}$ balances of figure 12† because the 'out-of-balance' term is the pressure–strain redistribution, whose behaviour is not well understood: there may again be anomalies in the highly curved region (waves can transport momentum) but the balance at $s = 61$ cm appears normal. The out-of-balance terms in the central part of each of the profiles of figure 11 are *not* attributable to the neglect of pressure transport (which must integrate to zero across the layer) but to inaccuracy in the measurement of

† Figure 12 (but not figure 10) is referred to rectangular Cartesian co-ordinates so that the 'rotation' term is absorbed into mean transport.

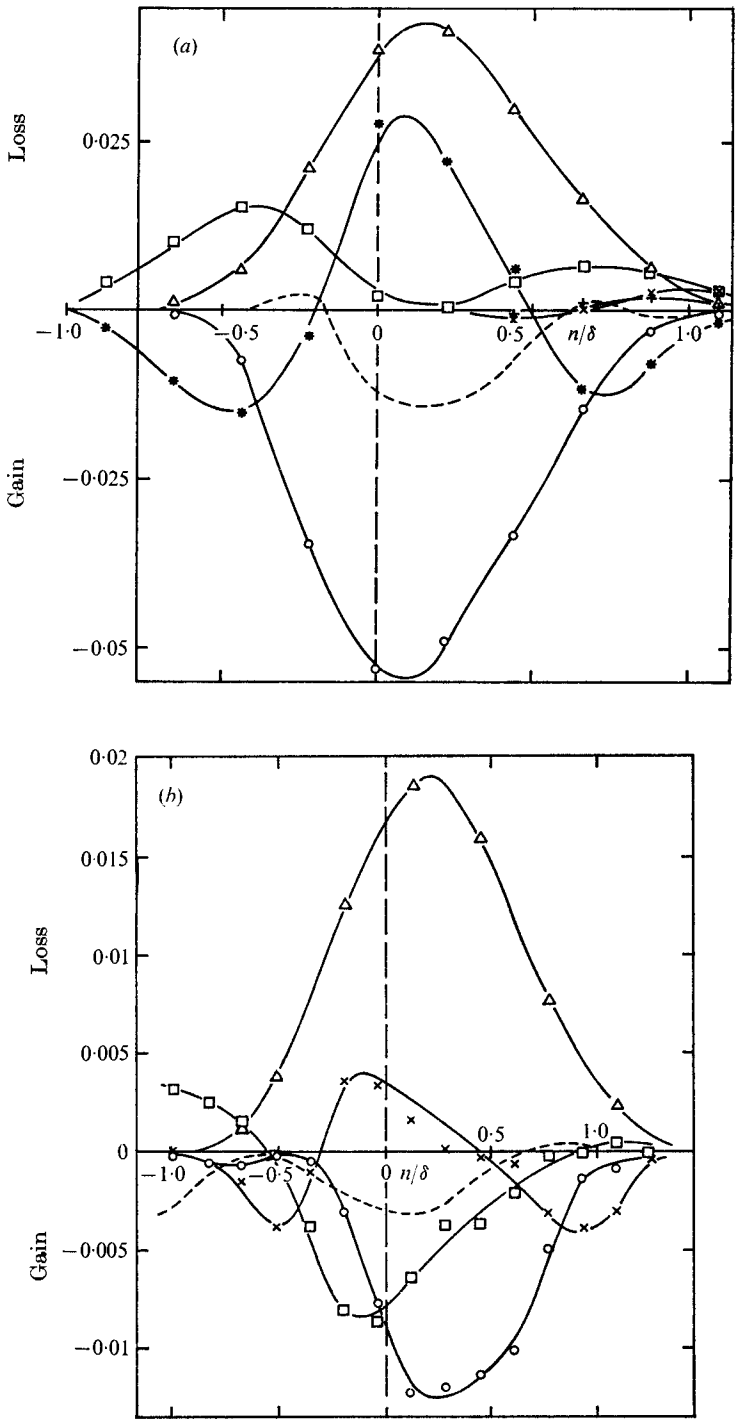

FIGURES 11 (*a*, *b*). For legend see page 292.

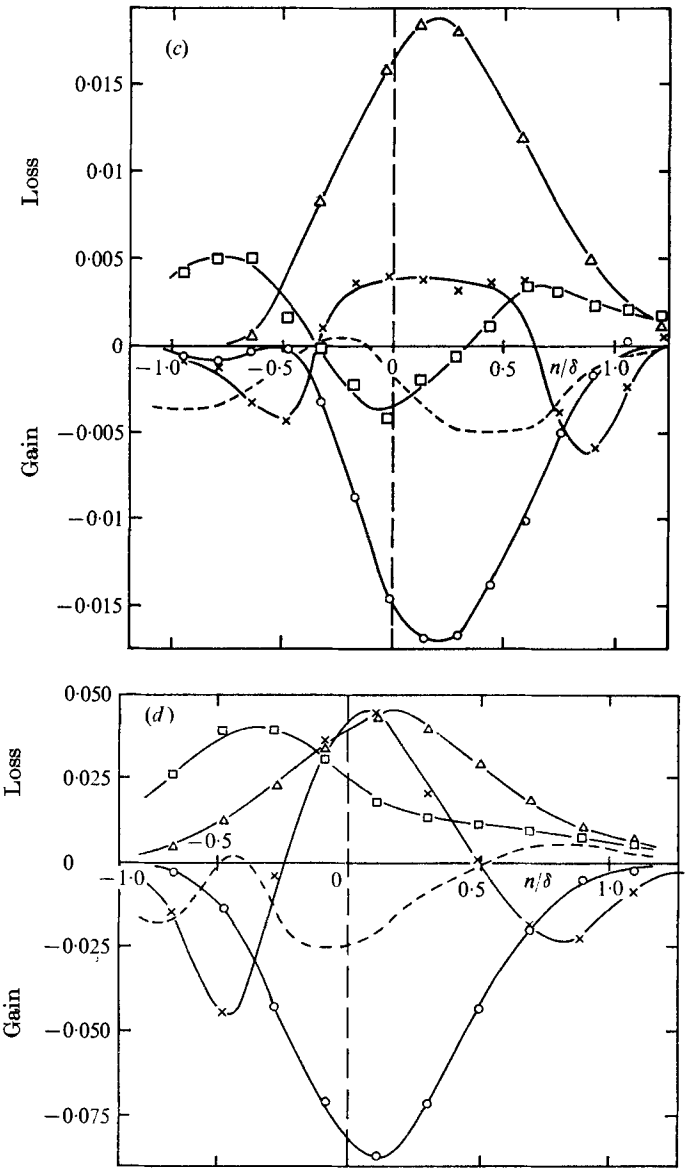

FIGURE 11. Profiles of terms in turbulent energy equation: for notation see figure 9. (*a*) Plane layer: +, normal-stress production; *, lateral triple-product diffusion; ×, longitudinal diffusion. (*b*) Curved layer, $s = 34{\cdot}4$ cm, $\theta = 50°$. (*c*) Curved layer, $s = 38{\cdot}8$ cm, $\theta = 60°$. (*d*) Curved layer, $s = 81{\cdot}5$ cm.

dissipation from frequency spectra (§ 2). The error is no worse in the curved layer than in the plane layer, and could have been reduced to zero by arbitrarily changing the multiplying constant in the inertial-subrange law to which the spectra were fitted. The error is small enough to be neglected in the present qualitative discussion, and the quantitative uncertainty is no greater than the discrepancies in, say, published measurements of $\overline{uv}$ in plane mixing layers. As in

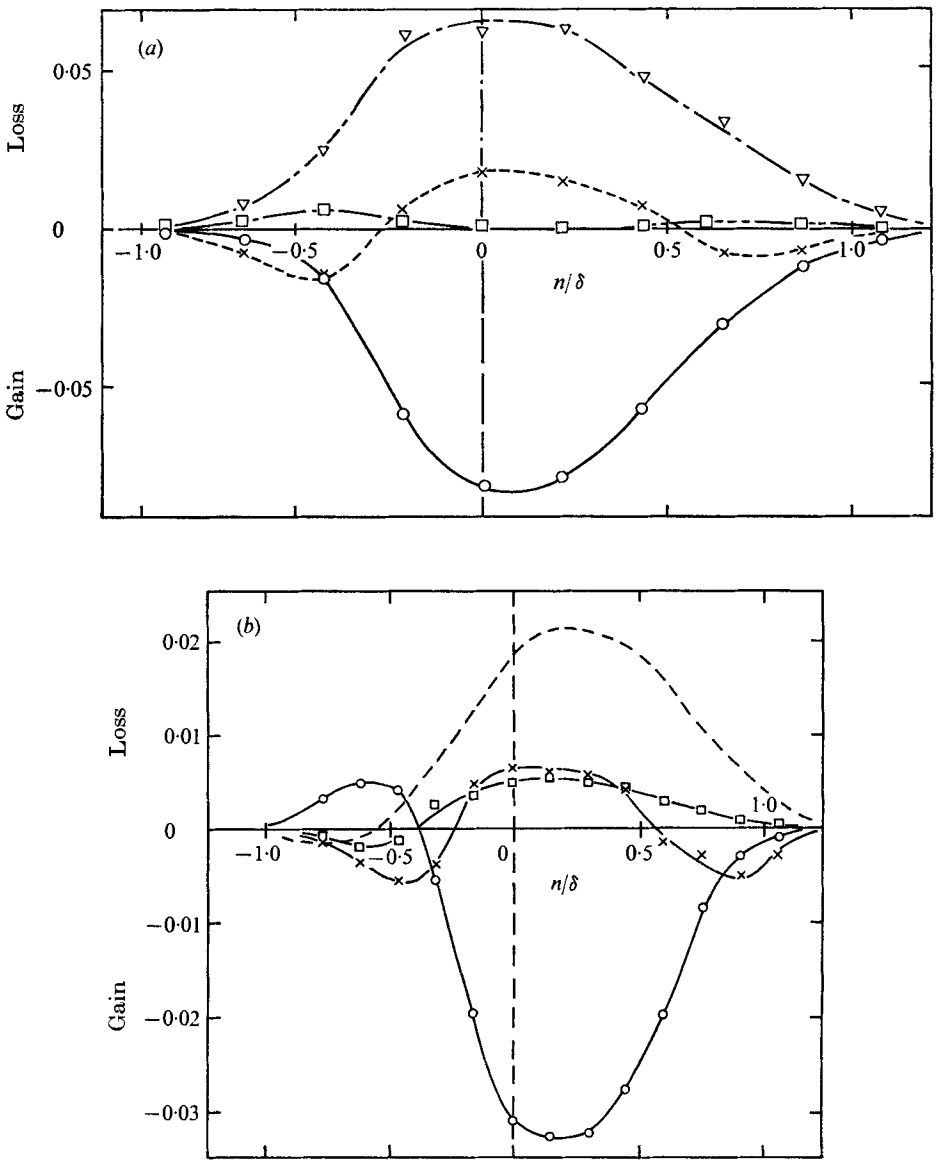

FIGURES 12(*a*, *b*). For legend see page 294.

the case of all the other measurements presented here, comparisons with our own plane-layer data provide a valid measure of curvature effects. The plane-layer values plotted at the right-hand sides of figures 9 and 10 have been corrected for the shift in apparent origin of the curved layer (no longer $s = 0$) and therefore vary slightly with s; the plane-layer values on the left are uncorrected.

The stabilizing effect of streamline curvature (figures 9 and 10), first in the pressure–strain term (Crow 1968) and then in the dissipation (spectral energy transfer), and assisted by the curvature-dependent generation terms, causes a

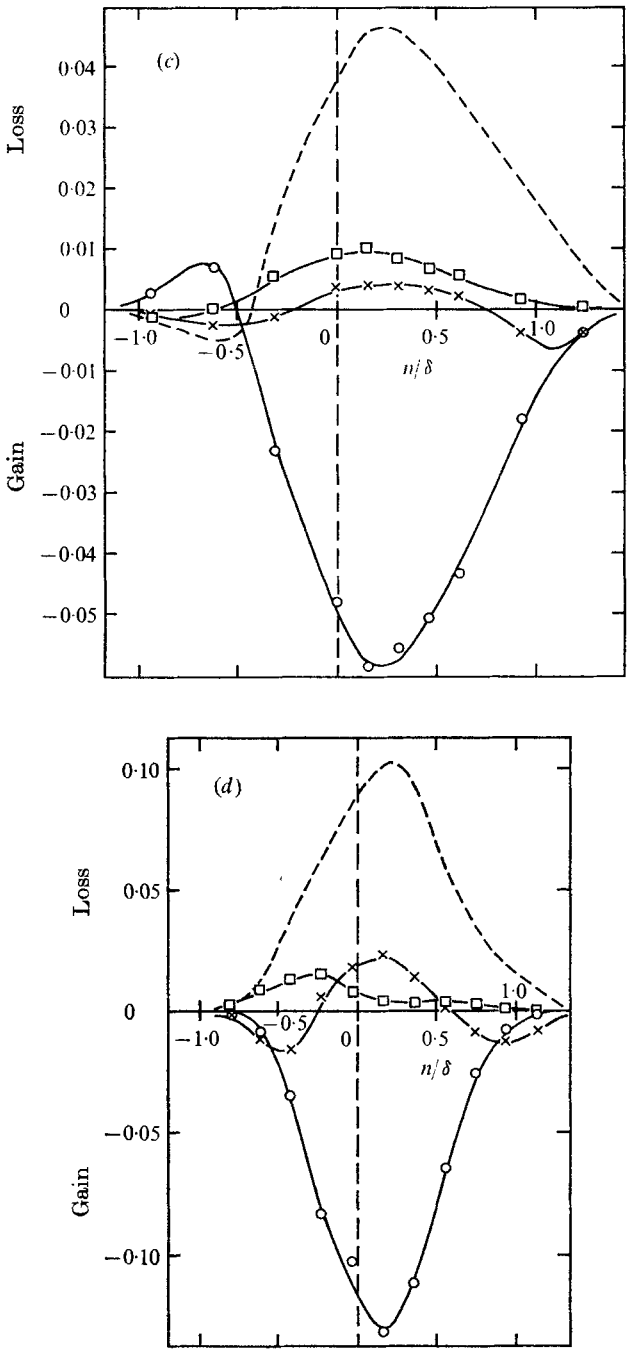

FIGURE 12. Profiles of terms in $\overline{uv}$ transport equation: for notation see figure 10. Here, rectangular Cartesian co-ordinates are used. (*a*) Plane layer. (*b*) Curved layer, $s = 29{\cdot}9$ cm, $\theta = 40°$. (*c*) Curved layer, $s = 38{\cdot}8$ cm, $\theta = 60°$. (*d*) Curved layer, $s = 61{\cdot}1$ cm.

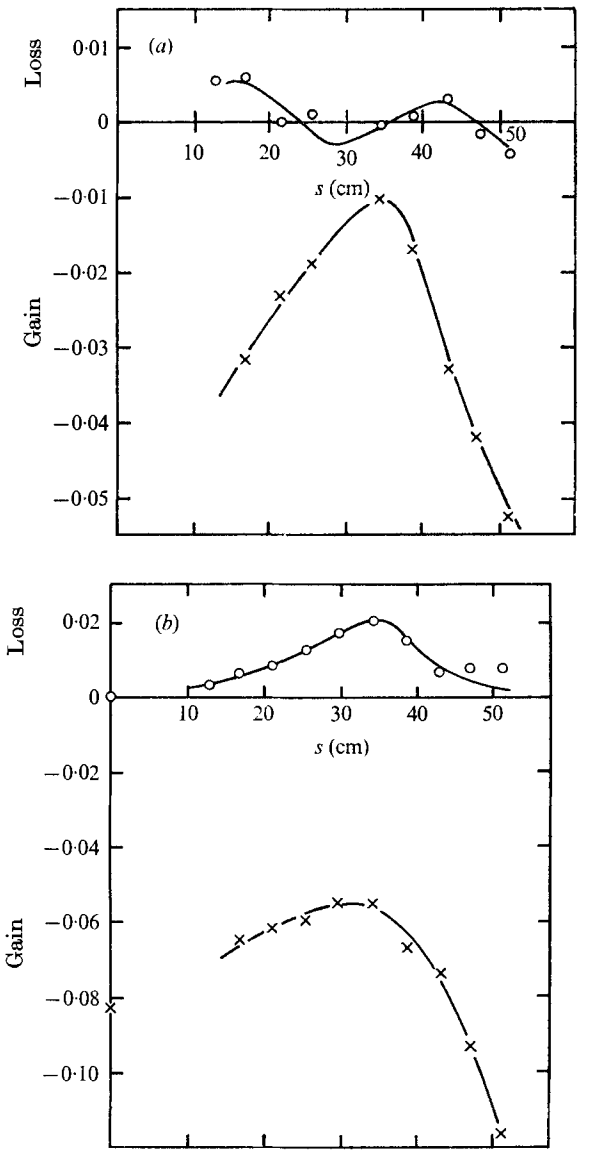

FIGURE 13. Small generation terms in the transport equations on the centre-line. (*a*) Turbulent energy equation: ×, shear production term; ○, normal-stress production (zero in plane layer). (*b*) $\overline{uv}$ transport equation: ×, shear generation term, $\overline{v^2}\partial U/\partial n$; ○, curvature term, $-\overline{u^2}U/R$.

decrease in shear stress and intensity, which has a self-perpetuating effect because of the resulting decrease in the generation terms. Mean transport down the longitudinal gradient partly compensates, *post hoc*, and loss to turbulent transport near the centre-line decreases. It does not seem profitable to discuss the transport equations for the triple products appearing in the turbulent transport terms because few of the terms in these equations have been measured in any

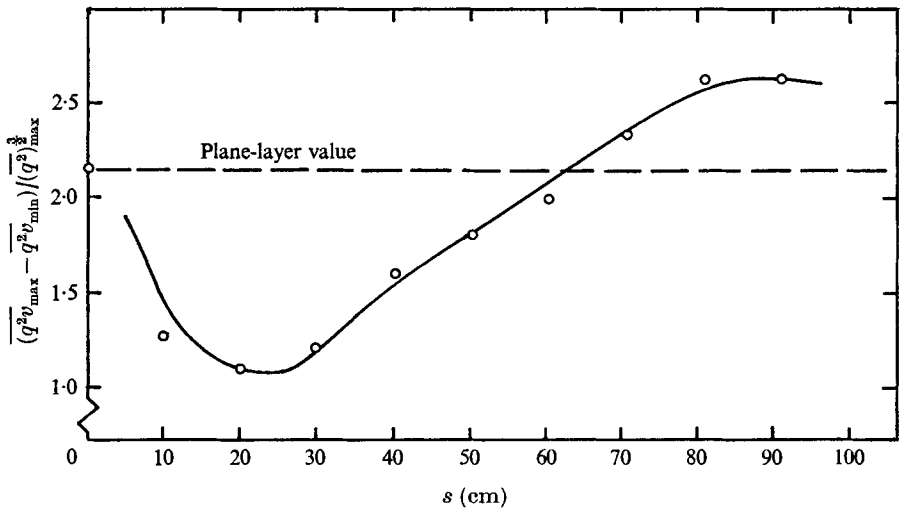

FIGURE 14. Relative strength of large eddies, $(\overline{q^2v}_{\max} - \overline{q^2v}_{\min})/(\overline{q^2})^{\frac{3}{2}}_{\max}$: 'max' implies maximum with respect to n at given s.

experiment. Figure 13 shows the size of some of the terms in the turbulent energy equation and the $\overline{uv}$ transport equation which would be neglected according to the thin-shear-layer approximation. Turbulent transport of turbulent energy in the longitudinal direction is quite significant but, like longitudinal stress gradients, its net effect on the flow downstream of the curved region is relatively small.

The fairly obvious statements in the last paragraph describe the flow behaviour up to about $s = 37$ cm (some 5 cm *after* the curvature (figure 2) starts to decrease). After this, the production of turbulent energy and the generation of $\overline{uv}$ increase rather rapidly while the turbulent transport remains small, though increasing, and the dissipation continues to *decrease* slowly until $s \simeq 45$ cm. A rapid, and again self-perpetuating, increase in intensity and shear stress ensues, continuing until the triple-product turbulent transport terms becomes large and drain energy away from the centre-line. The increase may be triggered by the rapid increase in the rate of shear strain $\partial U/\partial n - U/(R-n)$ as the curvature κ decreases, leading to an increase in the main energy production term. The reason why the increase is prolonged is apparently that the triple products are slow to grow. The energy production starts to rise as soon as the curvature starts to fall, but the rise in diffusion (turbulent transport of turbulent energy) is delayed for a streamwise distance of very roughly 3–4 shear-layer thicknesses, which is a typical large-eddy lifetime in this highly turbulent layer. A measure of the relative size of the triple-product term that appears in the turbulent transport of turbulent energy is plotted in figure 14: its increase after the minimum (which occurs *upstream* of the region of maximum curvature) is indeed rather slow although it crosses the plane-layer value at about the same streamwise position as $\overline{q^2}$ and $\overline{uv}$ do. Unfortunately this explanation of the overshoot ignores the effect of curvature on the pressure–strain term and the dissipation, which cannot be assessed:

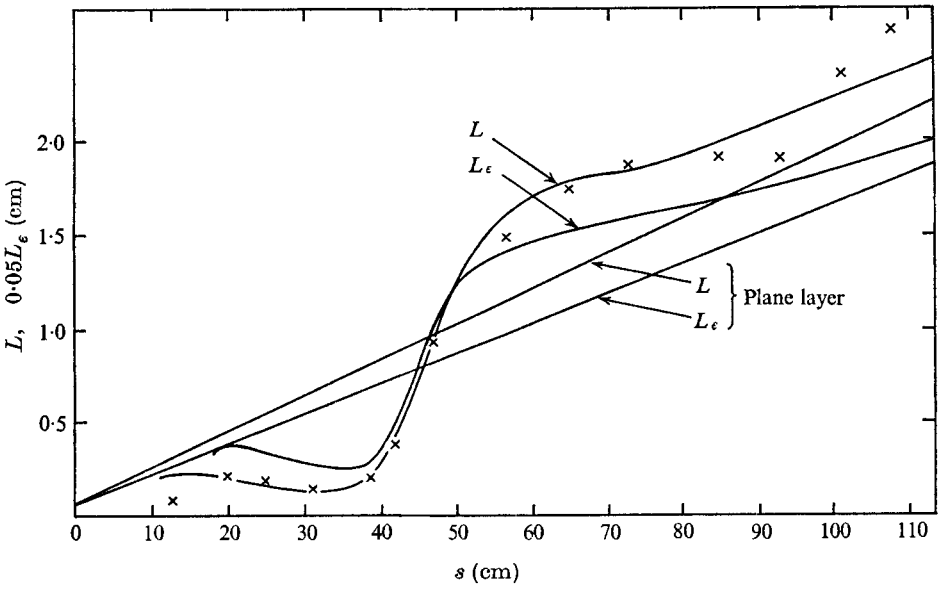

FIGURE 15. Dissipation length parameters.

the transport equation for the dissipation rate is even less accessible to measurement than that for the triple products.

A reflexion of the behaviour of the dissipation is the variation of the dissipation length scales $L \equiv (\overline{uv})^{\frac{3}{2}}/\epsilon$ and $L_\epsilon \equiv (\overline{q^2})^{\frac{3}{2}}/\epsilon$ along the centre-line (figure 15; the ratio L/L_ϵ is $a_1^{\frac{3}{2}}$, where a_1 is plotted in figure 7*b*). The spectacular variation of dL/ds and dL_ϵ/ds would not be greatly changed by adjusting ϵ to balance the turbulent energy equation on the centre-line. The relation between dissipation length scales and correlation length scales is not likely to be close, although L and L_ϵ are genuine length scales of the energy-containing motion in the sense that $\overline{uv}$, $\overline{q^2}$ and ϵ (equal to the spectral energy transfer through the top of the energy-containing range of wavenumbers) are all properties of the energy-containing motion. L is plotted against the flux Richardson number R_f (§4) in figure 16. As the curvature increases from zero, L at first increases linearly: the slope is probably not significant since the curvature is changing too rapidly for a 'Monin–Oboukhov' linear correction factor of the form

$$L/L_0 = (1+\beta R_f)^{-1}, \tag{6}$$

where β is a constant (Bradshaw 1969), to be valid. At large R_f the turbulence structure begins to saturate (L being necessarily positive, so that $1-L/L_0$ cannot exceed 1) but it is not certain that an asymptotic value of L has been reached by the time R_f begins to decrease. The hysteresis in the curve demonstrates the inadequacy of any correction factor based on a local R_f. We have tried a correction factor with R_f derived from a time-lagged value of the curvature (using a first-order ordinary differential equation with a time constant proportional to the shear-layer time scale) but, although the departure of L from the initial linear

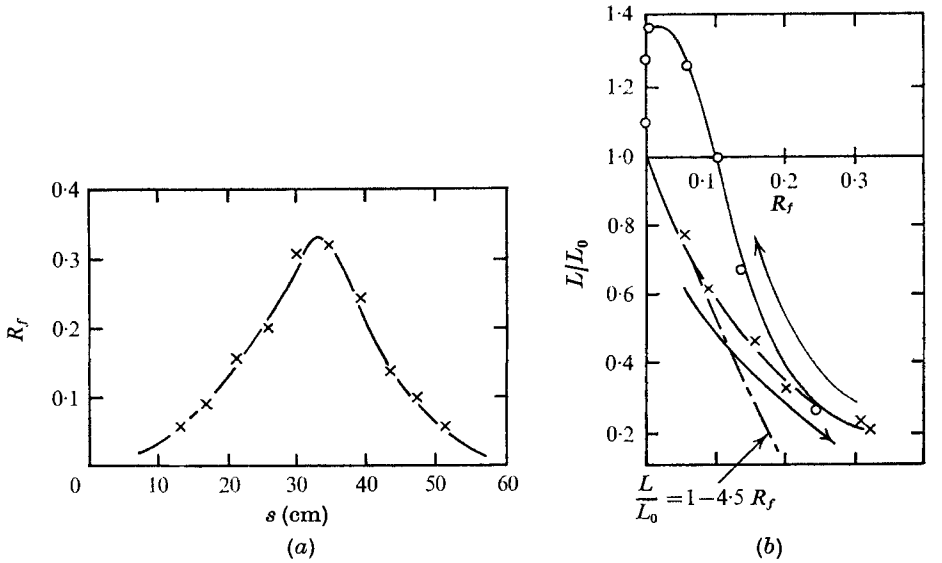

FIGURE 16. Flux 'Richardson number' R_f and its effect on L. L_0 is plane-layer value. (*a*) Streamwise variation of R_f. (*b*) Dependence of L on R_f: ×, curvature increasing; ○, curvature decreasing.

trend is postponed, the cusp at large R_f broadens into a loop and the discrepancy in the region of decreasing streamline curvature is even worse because the incipient overshoot in L resembles the effects of a phase advance rather than a phase lag. A second-order ordinary differential equation could in principle reproduce the observed behaviour of L but such a mechanistic approach is hardly justified.

The ratio of the extra rate of strain to the eddy time scale ($\frac{1}{2}R_f$ in the above notation) reaches a maximum of about 0·17 in the present flow (figure 16). This is a little large for the application of FTSL ideas, but, as seen above, they are helpful. For the quantitative application of rapid-distortion theory we require $\frac{1}{2}R_f \gg 1$ but, as pointed out by a referee, the concept of frozen turbulent vortex lines being distorted by the mean rate of strain is qualitatively useful even in the present case. The same referee has suggested that the rapid rise and overshoot of $\overline{uv}$ can be explained in terms of rapid-distortion theory (and, indeed, has already been predicted; Townsend 1970) but we do not feel that, in this flow, rapid-distortion theory could ever provide a complete explanation of the phenomenon and we have not attempted any quantitative comparisons. The modelling of the Reynolds-stress transport equations used recently by several authors (e.g. Launder, Reece & Rodi 1975) yields results close to those of rapid-distortion theory (e.g. Crow 1968) for large, suddenly applied rate of strain. Transport-equation calculation methods can in principle provide a satisfactory interpolation between the 'viscous' response of turbulence near local equilibrium after a prolonged rate of strain and the 'elastic' response to rapid distortion.

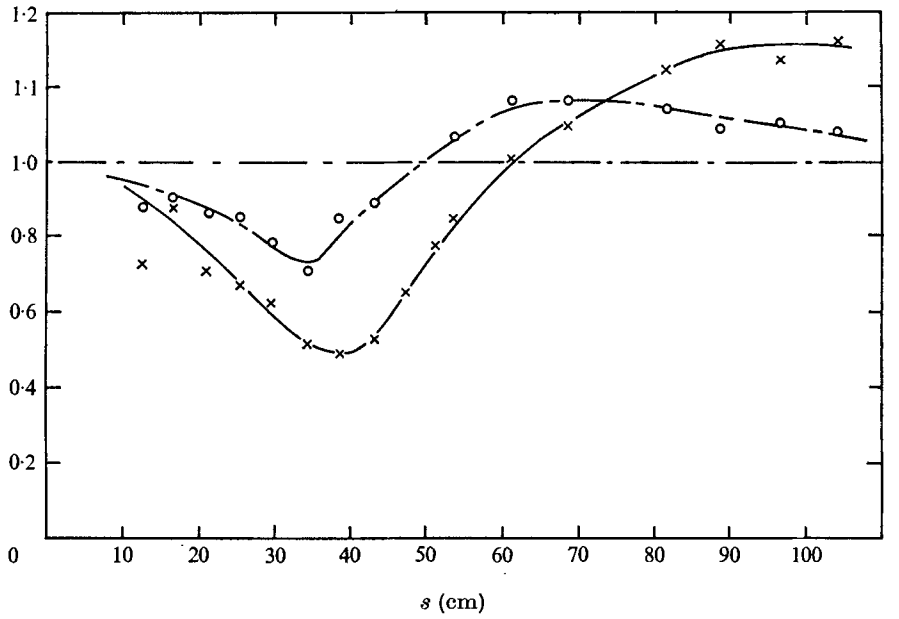

FIGURE 17. Principal stress and principal rate of strain. ×, maximum principal stress; ○, $\delta \times$ principal rate of strain. Both normalized by plane-layer values.

6. Implications for calculation methods

One practical application of turbulence research being the development of engineering calculation methods, the relevance of the present results to this application merits discussion. For the record, the maximum principal stress and the principal rate of strain are plotted against distance round the centre-line in figure 17. The graph does not itself demonstrate the invalidity of any local-equilibrium 'eddy viscosity' relation between the stress and strain rate (except the crudest of such relations based on the mean-flow scales U_{ref} and δ) but it does clearly show the lag in the response of Reynolds stress to a change in rate of strain – that is, the effect of 'history' or mean transport terms on the Reynolds stress. We have just demonstrated the inability of a simple Monin–Oboukhov factor to represent the effect of steamline curvature on the representative length scale L: in this case a contributory reason is the importance of turbulent transport of energy and other quantities in the direction normal to the stream-lines, which renders any local-equilibrium analysis invalid. Turbulent transport is more important in free shear layers than in wall flows, so that the present results may exaggerate the boundary-layer problem: however Young's measure-ments in a highly curved boundary layer indicate that turbulent transport will play an important part in some highly perturbed wall flows at least. Figures 18 (*a*)–(*d*) show the behaviour of the apparent eddy diffusivity and turbulent transport velocity for the triple products whose gradients are the main turbulent

transport terms in the turbulent energy equation and the shear-stress transport equation, respectively

$$\left.\begin{aligned} \nu_q &\equiv -\overline{q^2 v}(\partial \overline{q^2}/\partial y)^{-1}, \quad \nu_\tau \equiv -\overline{uv^2}(\partial \overline{uv}/\partial y)^{-1}, \\ V_q &\equiv \overline{q^2 v}/\overline{q^2}, \quad V_\tau \equiv \overline{uv^2}/\overline{uv}. \end{aligned}\right\} \tag{7}$$

The eddy diffusivities necessarily have singularities because the triple product does not pass through zero at the same point as the stress gradient but this, though spectacular, is not important enough for us to reject the use of eddy diffusivities for correlating data. A more serious objection is that even outside the neighbourhood of the singularities the diffusivities obey no simple rules and the behaviour of ν_τ is quite different from that of ν_q. The differences between the three ν_q profiles, plotted against n/δ, are reduced by scaling on $(\overline{q^2})^{\frac{1}{2}}$ rather than U_{ref} but the diffusivity for negative n at $s = 34{\cdot}4$ remains unnaturally small. One expects the general level of ν_q to be roughly proportional to $(\overline{q^2})^{\frac{1}{2}}_{\max}\delta$ simply because the profiles of $\overline{q^2}$ plotted against n/δ are roughly similar at different s positions, and it follows that changing the length scale from δ to L, or the related length $L_\epsilon \equiv (\overline{q^2})^{\frac{3}{2}}/\epsilon$, degrades the collapse. Therefore the common practice of scaling the eddy diffusivities on $(\overline{q^2})^{\frac{1}{2}}$ and L_ϵ is not acceptable here. However the FTSL concept allows one to use δ, rather than L or L_ϵ, as a length scale where appropriate, both in making the diffusivity dimensionless and in correlating it as a function of n/δ if necessary: δ is undoubtedly a relevant length scale if not a unique one.

The behaviour of the transport velocities V_q and V_τ is somewhat easier to grasp, although V_τ has a singularity near $n/\delta = -0{\cdot}5$ because of the negative loop in $\overline{uv}$ at $s = 34{\cdot}4$ (see figure 4(*g*): the same phenomenon is probably responsible, via a negative rate of turbulent energy production, for the anomalous behaviour of ν_q in the same region, but the most straightforward reasoning suggests that ν_q should be abnormally *large* in a region of low $\overline{q^2}$). The collapse of V_q and V_τ is improved by scaling V_q on $(\overline{q^2})^{\frac{1}{2}}_{\max}$ and V_τ on $(\overline{uv})^{\frac{1}{2}}_{\max}$: in this case no length scale is needed in the formula as a function of n/δ.

Clearly neither of the simple models of turbulent transport collapses the data accurately with any simple choice of scales but the transport-velocity model seems to be the better of the two in performance and is certainly the simpler to use.

A major term in the individual Reynolds-stress transport equations is the mean product of the pressure and the fluctuating rate of strain in the plane of the Reynolds stress concerned. In the present experiment the pressure–strain term $\overline{p'(\partial u/\partial n + \partial v/\partial s)}$ in the uv transport equation has been obtained by difference. This is not the place for exploration of different schemes for modelling this term but one common assumption seems to be definitely contradicted: this is the 'anisotropy' assumption that the above pressure–strain term is proportional to uv divided by a time scale of the turbulence. Choosing the time scale as $L/(\overline{uv})^{\frac{1}{2}}$ in conformity with FTSL ideas implies that the pressure–strain term should be directly proportional to the dissipation, and comparison of figures 9 and 10 shows that it is not. An alternative choice for the time scale is $L_\epsilon/(\overline{q^2})^{\frac{1}{2}}$, implying pressure–strain $\propto \epsilon\overline{uv}/\overline{q^2}$; however $\overline{uv}/\overline{q^2}$ (figure 7*b*) returns to its plane-layer value

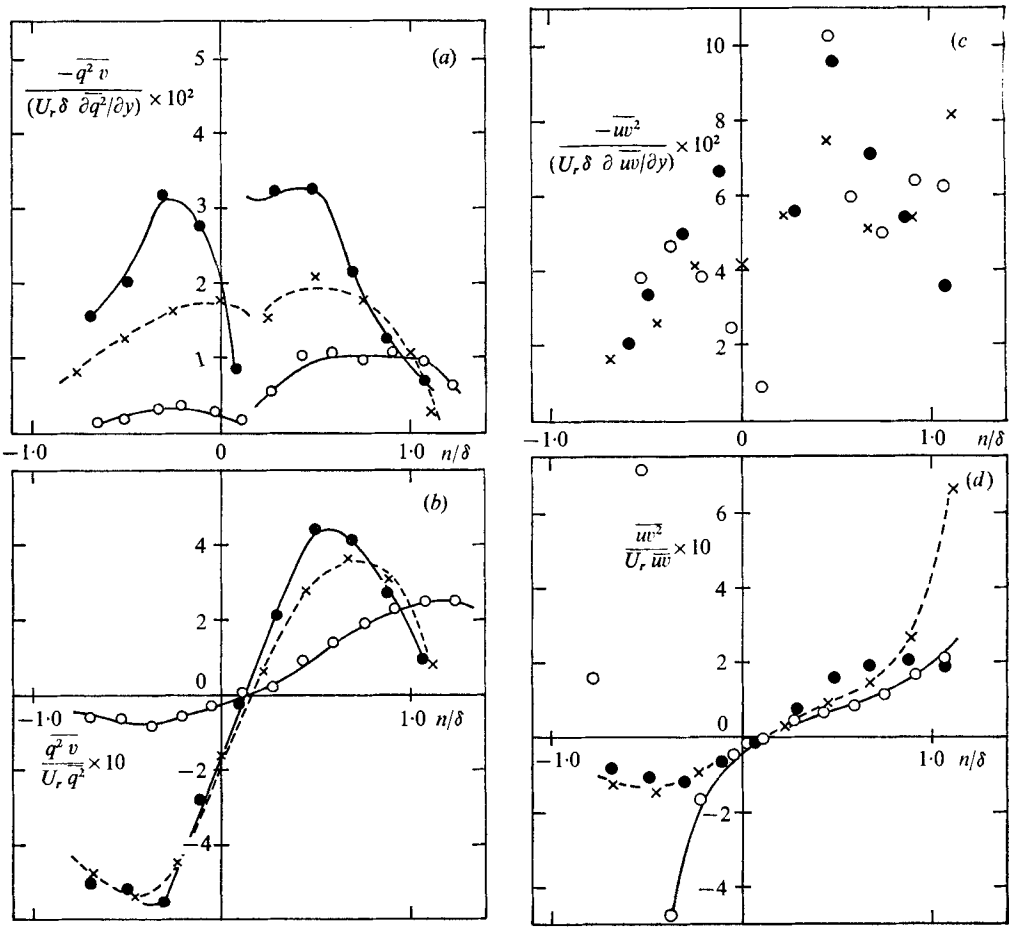

FIGURE 18. Diffusivity and bulk-convection velocity derived from triple-product transport terms. ●, plane layer; ○, $s = 34{\cdot}4$ cm; ×, $s = 81{\cdot}5$ cm. (*a*) Turbulent energy diffusivity $\nu_q/(U_r\delta)$. (*b*) Turbulent energy bulk-convection velocity V_q/U_r. (*c*) Shear-stress diffusivity $\nu_\tau/U_r\delta$. (*d*) Shear-stress bulk-convection velocity V_τ/U_r.

by $s \simeq 60$ whereas the ratio of pressure–strain to dissipation in the later part of the curved flow is almost 1·5 times that in the plane layer. Use of δ as a scale instead of L or L_ϵ would not greatly improve agreement in the later part of the flow, where L is no more than 1·1–1·2 times the plane-layer value. The alternative models for the pressure–strain term include, in addition to the 'anisotropy' term, a term proportional to the mean strain rate, but the choice of the factor multiplying the mean strain rate is not unique (Launder *et al.* 1975) so such models can be tested only individually and not as a class.

A number of recent calculation methods include empirically modelled partial differential 'transport' equations for an eddy length scale or its equivalent, as well as for Reynolds stresses or their equivalents. Sometimes the exact transport equation for dissipation is modelled but the result can be converted into an equation for L or L_ϵ by using the definitions of those quantities together with the

transport equations for $\overline{uv}$ or $\overline{q^2}$. The simplest form of length-scale transport equation in a two-dimensional plane shear layer (retaining s, n co-ordinates for simplicity) is (Bradshaw & Unsworth 1973)

$$U\frac{\partial L}{\partial s}+V\frac{\partial L}{\partial n}=c_1 L\frac{\partial U}{\partial n}-\frac{\partial}{\partial n}(V_L L)+c_4|\overline{uv}|^{\frac{1}{2}}, \tag{8}$$

where c_1 and c_4 are dimensionless 'constants' (or functions) and V_L is the transport velocity of L. Further refinements of the sort implied in the current literature are unlikely to affect the following discussion.

The first term on the right-hand side is small in most existing model length-scale equations and we shall assume it to be negligible here. We shall also tentatively assume that L is independent of n, which is normally a good approximation for energy-containing length scales in free shear layers, and integrate (8) across the layer to remove the turbulent transport term. The result is

$$dL/ds = c\int|\overline{uv}|^{\frac{1}{2}}\,dn/4\int U\,dn, \tag{9}$$

which we may approximate by

$$dL/ds = c'(|\overline{uv}_{\max}|/U^2_{\text{ref}})^{\frac{1}{2}} \tag{10}$$

for shear layers whose shear-stress and velocity profiles have nearly constant shape. Clearly (10) implies that L increases monotonically with s. For the plane mixing layer, $c' \simeq 0{\cdot}23$ according to the present results. An obvious extension of (8) to a shear layer with an extra strain rate e involves adding a term $c_5 L_e$ to (8). With $e = U/R$ the corresponding addition to (10) is $c_5'\,L/R$. With the example of the 'Monin–Oboukhov' formulae in mind we may expect c_5 to be much greater than c_1, so that the extra term in (8) may be significant even if c_1 is small. However it is easy to see that no *constant* c_5' can account for the behaviour of L in the curved mixing layer (figure 15), in particular the very large value of dL/ds near $s = 50$ cm, where $\overline{uv}_{\max}$ is still well below the plane-layer value while the curvature-dependent term is still significant and tending to reduce L. We conclude that the addition, to a length-scale equation of the type (8), of terms depending on the *local* value of the extra strain rate is no more successful in reproducing the present result than equation (6), the 'Monin–Oboukhov' correction to the shear-stress equation. Other choices of length scale may be better behaved than L, but L and L_e are the most commonly used in calculation methods.

Now there are numerous weak points in the above argument, notably the assumption that L remains independent of n in the curved layer, but even with a generous allowance for uncertainty about the smallness of c_1 and the n-wise variation of L it is difficult to see how any simple extension of (8) with constant values of the c's could reproduce a value of dL/ds three or four times that in the plane layer. One is forced towards the conclusion that a further level of allowance for history effects is necessary – for instance 'transport' equations for one or more of the empirical constants, or the turbulent transport velocity, in (8). This takes one so far from measurable quantities that one would at present have little confidence in a calculation method employing such concepts, unless some

breakthrough in physical understanding can be made. Such a breakthrough could result only from a more detailed study of length scales in complex flows than we have been able to make in the present case.

7. Conclusions

The stably curved mixing layer of figure 1 is a flow which is perturbed from a self-preserving state by a short region of extra strain rate $\partial V/\partial x$, which reaches a maximum value of about $-0{\cdot}2\partial U/\partial y$; the flow then relaxes back to the same self-preserving state. The thin-shear-layer approximation is not valid, but the 'fairly thin shear layer' concept has been shown to be useful: even in this strongly perturbed flow we have been able to define a shear-layer direction, and in axes along and normal to this direction the terms in the mean-motion equations which would be neglected in a thin shear layer are small enough to be *approximated*. This FTSL concept should be useful in nearly all flows with significant Reynolds-stress gradients. Although the explicit extra terms in the equation for the transport of momentum and Reynolds stress are fairly small, the effects of the extra strain rate on the turbulence structure are large. The Reynolds stresses and other turbulence quantities decrease in the region of maximum curvature, as expected, but then overshoot the self-preserving values before the final relaxation. This appears to be a new phenomenon in turbulent flow, and has also been observed in a highly curved boundary layer. Apparently, suppression of the triple products which effect turbulent transport permits an unusual increase in turbulent intensity in the central part of the layer where energy production is greatest: the main contribution to the triple products comes from the large eddies, which have the longest time scales and therefore take longest to recover from the effects of stabilizing curvature. The results have been discussed in detail with special reference to engineering calculation methods. The simple local-equilibrium correction formulae which suffice to predict the effects of small continued curvature do not reproduce the observed results, and an allowance for rate-of-strain history, successfully used to extend the correction formulae to cases of small but rapidly varying curvature, make the agreement even worse. Even the more refined empirical 'transport' equations for the eddy length scale seem to be essentially incapable of reproducing the decrease in length scale observed in the region of maximum curvature. Finally, the two common models of turbulent transport, the gradient-diffusion model which defines an eddy diffusivity and the bulk-convection model which defines a transport velocity, are shown to give a poor correlation of the measured triple products: the simpler bulk-convection model seems to be the more satisfactory of the two. The initial contribution of the present work to the development of calculation methods is largely a negative, cautionary one. However the measurements should be useful in the formulation and testing of more refined turbulence models, representing as they do one of the most strongly perturbed shear layers likely to be found in practice.

We are grateful to the Donald Campbell Memorial Trust for supporting this work and for the award of a fellowship to one of us (I.P.C.) and to several colleagues and former colleagues, notably Dr A. Brandt, Dr M. E. Davies and Dr R. B. Dean, for helpful discussions and for assistance with data reduction.

REFERENCES

BRADSHAW, P. 1969 *J. Fluid Mech.* **36**, 177.

BRADSHAW, P. 1971*a* *AGARD Conf. Proc.* no. 93.

BRADSHAW, P. 1971*b* *An Introduction to Turbulence and Its Measurement.* Pergamon.

BRADSHAW, P. 1973 *AGARDograph*, no. 169.

BRADSHAW, P. 1974 *J. Fluid Mech.* **63**, 449.

BRADSHAW, P. 1975 *J. Fluids Engng, Trans. A.S.M.E.* **97**, 146.

BRADSHAW, P., DEAN, R. B. & MCELIGOT, D. M. 1973 *J. Fluids Engng, Trans. A.S.M.E.* **95**, 214.

BRADSHAW, P., FERRISS, D. H. & JOHNSON, R. F. 1974 *J. Fluid Mech.* **19**, 591.

BRADSHAW, P. & MURLIS, J. 1974 *Imperial College Aero Rep.* no. 74–04.

BRADSHAW, P. & UNSWORTH, K. 1973 *Imperial College Aero Rep.* no. 73-05.

BRADSHAW, P. & UNSWORTH, K. 1974 *Imperial College Aero Rep.* no. 74-02.

BRADSHAW, P. & WONG, F. Y. F. 1972 *J. Fluid Mech.* **52**, 113.

BRANDT, A. & BRADSHAW, P. 1972 *Imperial College Aero Rep.* no. 72–11.

BREDERODE, V. DE & BRADSHAW, P. 1974 *Imperial College Aero Rep.* no. 74–06.

BROWN, G. L. & ROSHKO, A. 1974 *J. Fluid Mech.* **64**, 775.

CASTRO, I. P. 1973 Ph.D. thesis, Imperial College, London.

CHANDRSUDA, C. & BRADSHAW, P. 1975 *Imperial College Aero Rep.* no. 75–03.

CROW, S. C. 1968 *J. Fluid Mech.* **33**, 1.

DEAN, R. B. 1974*a* Ph.D. thesis, Imperial College, London.

DEAN, R. B. 1974*b* Paper presented at *5th Australasian Conf. on Hydraul. & Fluid Mech., Canterbury, New Zealand.*

GILES, J. A., HAYES, A. P. & SAWYER, R. A. 1966 *Aero. Quart.* **17**, 201.

GRANT, H. L., STEWART, R. W. & MOILLIET, A. 1962 *J. Fluid Mech.* **12**, 241.

GUITTON, D. E. 1970 Ph.D. thesis, McGill University, Montreal.

LAUNDER, B. E., REECE, G. J. & RODI, W. 1975 *J. Fluid Mech.* **68**, 537.

LIEPMANN, H. W. & LAUFER, J. 1974 *N.A.S.A. Tech. Note*, no. 1257.

MERONEY, R. N. 1974 *Imperial College Aero Rep.* no. 74–05.

MOREL, T., TORDA, T. P. & BRADSHAW, P. 1973 *N.A.S.A. Special Publ.* SP-321.

PAO, Y-H. 1969 In *Clear Air Turbulence and Its Detection* (ed. J. H. Olsen, A. Goldburg & M. Rogers), p. 73. Plenum.

SO, R. M. C. & MELLOR, G. L. 1972 *N.A.A.S. Contractor Rep.* CR-1940.

SO, R. M. C. & MELLOR, G. L. 1973 *J. Fluid Mech.* **60**, 43.

TOLLMIEN, W., SCHLICHTING, H. & GÖRTLER, H. 1961 *Ludwig Prandtl Gesammelte Abhandlungen.* Springer.

TOWNSEND, A. A. 1970. *J. Fluid Mech.* **41**, 13.

WEBER, D. P. 1974 Ph.D. thesis, University of Illinois at Urbana-Champaign.

WINANT, C. D. & BROWAND, F. K. 1974 *J. Fluid Mech.* **63**, 237.

WYGNANSKI, I. & FIEDLER, H. 1970 *J. Fluid Mech.* **41**, 327.

WYNGAARD, J. C. 1967 Ph.D. thesis, Pennsylvania State University.

WYNGAARD, J. C. 1968 *J. Sci. Instrum.* **1** (2), 1105.

WYNGAARD, J. C., TENNEKES, H., LUMLEY, J. L. & MARGOLIS, D. P. 1968 *Phys. Fluids*, **11**. 1251.